THE BELL SYSTEM TECHNICAL JOURNAL
Vol. 53, No. 10, December 1974
Printed in U.S.A.

L5 SYSTEM:

Transmission Networks and Magnetic Components

By J. L. GARRISON, A. OLSEN, JR., and T. H. SIMMONDS, JR.

(Manuscript received March 4, 1974)

The development of transmission networks and magnetic components for the L5 system represents the largest network development project of its type ever undertaken within the Bell System. Over 200 different coded designs of networks, requiring in excess of 40 man-years of effort, were required to meet the frequency-selective and signal-shaping requirements of the system. Despite this effort, neither systems requirements nor systems schedules could have been met without significant contributions from allied technologies. This article identifies those technologies and describes design techniques that have advanced the state-of-the-art capabilities in transmission network and magnetic component design.

I. TRANSMISSION NETWORKS

1.1 Introduction

As in other analog systems, transmission networks of the L5 Coaxial-Carrier Transmission System perform the indispensable functions of frequency selection and signal shaping. Without the filtering functions provided by certain of these networks, the basic multiplexing arrangements on which the system depends could not be realized, nor could the various fault-locating, equalizing, regulating, and switching pilots be effectively separated from the message portion of the line signal. Similarly, without use of the wide variety of equalizers provided, the amplitude distortions introduced as the signal traverses the line could not be as effectively corrected. Examples of such equalizers include *line-build-out* (LBO) *networks* to compensate for cable spans shorter than the nominal one-mile spacing, *fixed equalizers* to compensate for time-invariant and predictable effects, and *adjustable equalizers* to reduce the unpredictable, statistical variations of the system.

To complete a listing of system functions performed by the transmission networks of the L5 system would require a tabulation of all major system functions. Over 200 transmission networks, requiring in excess of 40 man-years of effort and representing the largest network development of its type ever undertaken within the Bell System, were developed for L5. Despite this large and sustained effort, the required designs could not have been produced without significant advances in computer-aided design, precision measurement, magnetic components, and monolithic crystal filters. The purpose of the transmission networks section of this paper is to identify those technologies that have influenced network developments for the L5 system and to describe certain techniques that have advanced the state-of-the-art capabilities in network design.

1.2 Network technology

The majority of networks for the L5 system were developed using classical network synthesis procedures. Insertion-loss synthesis techniques were used exclusively for filter realization, Bode's semi-infinite slope approximation for LBO networks, cable equalizers and artificial lines, and constant-resistance bridged-T networks, in various topologies, for fixed and variable amplitude equalizers. State-of-the-art advances stemmed primarily from the stringent requirements imposed by the system rather than from network theoretic developments. Strong interaction between systems and network engineers, in frequency allocation and the setting of reasonable guard bands, assisted greatly in the problem of filter realizability. In practically all cases, developing techniques for reducing circulating currents, and developing practical design procedures for the compensation of parasitics were a necessary adjunct to the physical realization of manufacturable networks.

1.3 JMX modulation filters

The development of modulation filters for the jumbogroup multiplex terminal (JMX)[1] is typical of that for the many filter designs produced for the L5 system. Figure 1 is a simplified block diagram of the JMX terminal as viewed by a networks designer. The modulation scheme is typical of most analog multiplex systems except for the multiple-modulation steps. Although the double and triple steps of modulation increase the number of filter designs required, they reduce the complexity of the individual filters. The final circuit and networks objectives were the result of extensive discussions between systems and

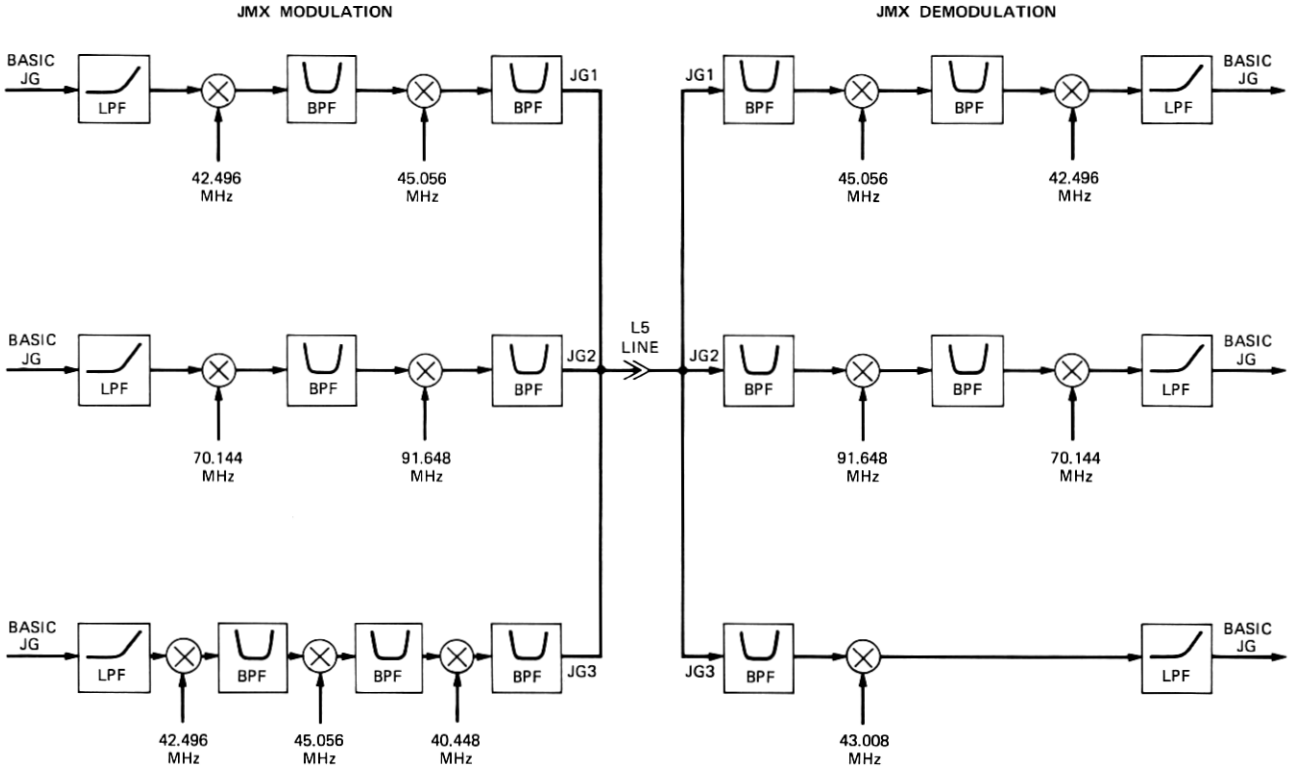

Fig. 1—Simplified block diagram of JMX terminal emphasizing transmission networks.

networks engineers with the goal of optimizing the trade-off between frequency-spectrum utilization and the setting of adjacent jumbogroup guard bands.

As a result of such discussions, typical filter transition bands approximated a reasonable 10 percent, which allowed the use of small slug-tuned, air-core inductors having a maximum quality factor (Q) of approximately 150. All 14 of the filter designs—10 complex bandpass, 3 low-pass, and 1 low-pass-high-pass filter—are equal-ripple insertion-loss designs. The degree of the filters ranged from a minimum of $n = 7$, for a simple low-pass filter having a relatively low stopband objective and a wide transition band, to a maximum of $n = 20$, for a more difficult bandpass design having an 80-dB discrimination objective across the unwanted sideband. Figures 2 and 3 show the schematic diagram and measured characteristics, respectively, of one of the more complex bandpass filters.

The initial design phases were concerned with the optimization of the filter designs for practical element values, low passband delay distortion, good out-of-band performance, and acceptable inband return loss. Versatile insertion-loss synthesis, pole-placing, and analysis programs were available.[2] Some of the features of the programs found particularly useful during the design stage were: (*i*) the ability to choose arbitrary stopbands with Chebychev passband behavior, (*ii*) the ability to order loss peak removal to optimize element values, and (*iii*) the automatic computation of network characteristics subsequent to the solution of the synthesis problem.

Extensive use was also made of available programs to minimize the delay distortion contributed by the modulation filters for any future application of the JMX terminal to data systems. Theoretical cutoffs were placed as far into the transition region as possible without unduly increasing the degree of the filters or making the element values impractical. This modification of the designs achieved up to a 50-percent reduction in delay distortion over the desired portion of the passband with only a 10-percent increase in the complexity of the filters.

As a result of the JMX modulation arrangement, the carrier, in many cases, fell close to the passband edges, making it impossible (with the extended theoretical cutoffs) to adequately suppress the carrier leak. Quartz crystals, as shown in the schematic of Fig. 2, were therefore introduced in various shunt branches to suppress the unwanted carrier. Highly stable, high-Q, AT-cut crystals, designed for maximum suppression of unwanted responses, were used. Other components

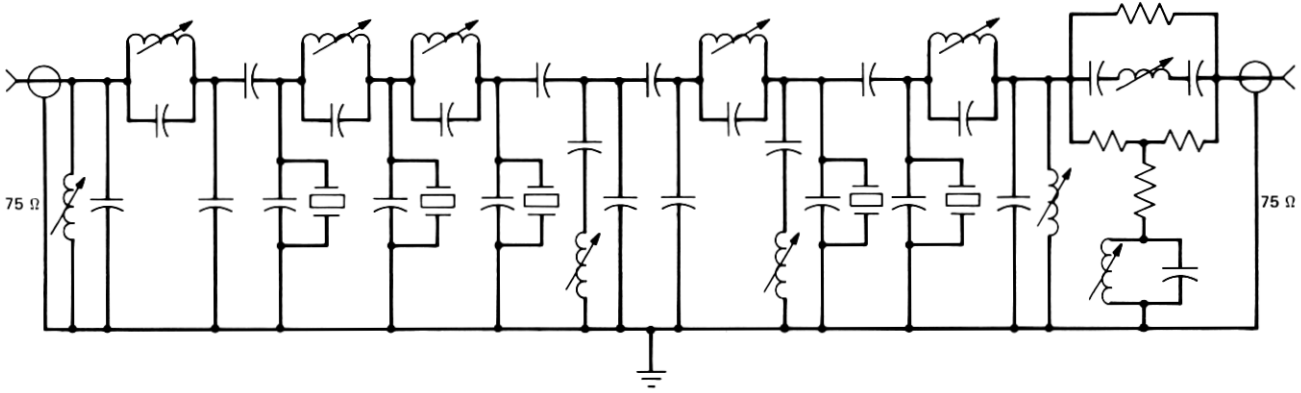

Fig. 2—Network schematic of typical JMX bandpass filter.

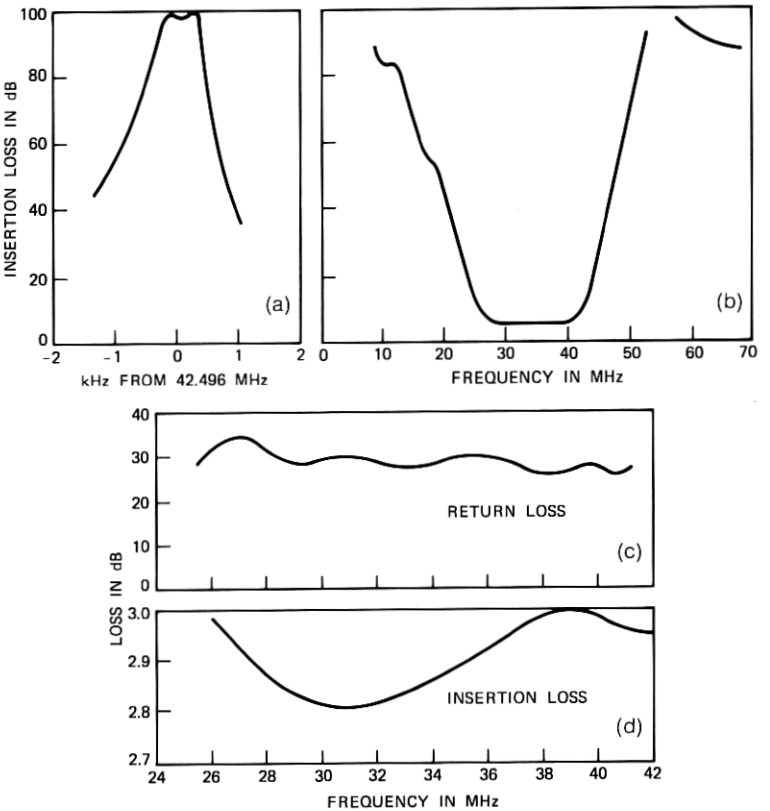

Fig. 3—Characteristics of typical JMX bandpass filter. (a) Component of loss contributed by crystals at 42.496 MHz. (b) Stopband loss. (c) Return loss. (d) Passband loss.

included adjustable air-core inductors and dipped-mica and tubular capacitors. These components were mounted on printed wiring boards (PWB's) and packaged in sealed enclosures.

Laboratory development of the JMX networks was a difficult and lengthy process because of the wide bandwidths and high frequencies involved. Precision scanning network analyzers were used widely in the initial stages of development, but in all instances the computer-operated transmission-measuring set[3] (COTMS) was used for final characterization.

1.4 Monolithic crystal bandpass filters

Monolithic crystal filters[4] have found wide application in the L5 system as narrow-band pick-off filters and as wide-passband band-

elimination structures. The monolithic crystal filter was first introduced in the Bell System plant as simple two-resonator bandpass filters for carrier-supply applications[5] in the L4 coaxial system. For the L5 system, over 40 designs, ranging in frequency from less than 3 MHz to nearly 100 MHz, were required for both bandpass and band-elimination applications. To cover this frequency range, fundamental and third-overtone crystal designs were necessary, and multiresonator filtering arrangements were provided to meet the high out-of-band suppression requirements.

The monolithic crystal filter, in its most elementary form, consists of a quartz plate with an array of two-electrode pairs placed on its major surfaces, with each pair establishing a resonator system. The resonators are acoustically coupled via the elastic quartz plate. If the quartz plate, electrode pairs, and acoustic coupling are properly proportioned, a self-contained, two-port piezoelectric device, having prescribed filtering characteristics, results. Higher-order filter functions may be obtained by deposition of multielectrode pairs on an extended quartz plate, with adjacent resonators acoustically coupled. As an extension of this arrangement, multiple quartz plates may be used, with adjacent resonators (on facing quartz plates) coupled electrically (capacitively). A third alternative, the composite monolithic crystal filter, uses LC filter sections to couple individual two-resonator monolithics. The latter approach was used exclusively in the design of more than 30 monolithic crystal bandpass filters for L5 applications. Impedance-matching sections necessarily were included in these designs to match the impedances of the coupled-resonator designs to specified source and load impedances. This combination of LC coupling networks, LC impedance-matching networks, and two-resonator monolithics led to the concept of the monolithic crystal filter (MCF) as a two-port, building-block device available for inclusion in some larger frequency-selective network.[6,7]

Before describing those methods of design peculiar to the composite MCF, a more detailed summary of methods of deriving higher-order filter functions is required. Figure 4 shows the three different techniques described above. In each instance, an impedance-matching network is indicated at the input and output ports of the networks. These may or may not be required. Figure 4a shows the multiresonator MCF on a single piece of quartz with the interresonator coupling supplied by the built-in acoustic coupling properties of the device itself. To avoid acoustic coupling of certain unwanted modes, the approach indicated in Fig. 4b is sometimes advisable. In this instance, the single plate of Fig. 4a has been split into two parts and the facing

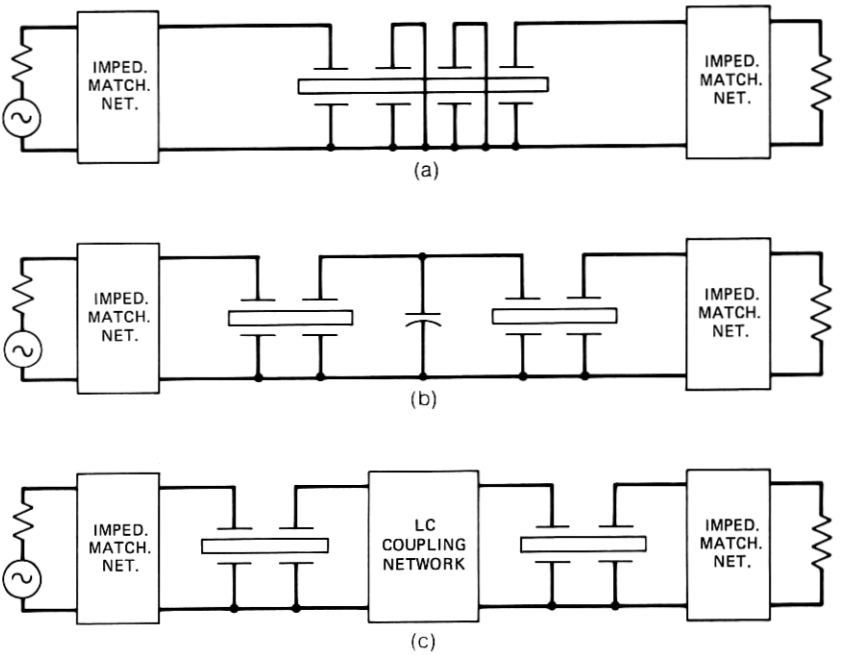

Fig. 4—Methods of deriving higher-order filter functions. (a) Multiorder monolithic filter with acoustic interresonator coupling. (b) Multilithic filter with acoustic and electrical interresonator coupling. (c) LC network coupling of two identical MCF's.

pairs of electrodes electrically coupled by the capacitor are shown in the figure. The present design of the A6 channel-bank filters[8] uses this technique. The third method of realization is represented in the schematic of Fig. 4c. This schematic emphasizes the concept of the MCF as a two-port, building-block device employing supplementary LC filter sections (coupling networks) and impedance-matching networks for realization of a particular transfer function. In all three examples shown in Fig. 4, the classical work of Dishal[9] provides closed-form solutions in the design of narrow-band bandpass filters to exact amplitude characteristics.

In view of the importance of the building-block concept to the design of composite MCF's, devices and filter sections required for filter realization are shown in Figs. 5 and 6. Emphasizing the role of the MCF as a two-port device in composite-filter design, schematics for the basic and reversed-phase connections of a symmetrical, two-resonator MCF and their equivalent circuits are shown in Fig. 5. The associated LC networks required in a composite filter design are shown

in Fig. 6. These include both impedance inverters and impedance-matching networks. The impedance inverters are shown in their T- and pi-configurations and consist of positive and negative capacitive elements. In the final network design, the negative capacitances shown in the figure are either absorbed in positive capacitances existing within the network, or are approximated in a narrow-band sense by inductances.

The impedance-matching networks of Fig. 6 are shown in their L-configurations. It is important to note that the shunt elements of these networks must also be designed to "absorb" the input or output static capacitances of the associated MCF's.

Given the equivalent circuits of Figs. 5 and 6, design techniques applicable to multiresonator bandpass filters become readily apparent. A familiarity with the theory of coupled-resonator design, however, is assumed. References 9, 10, and 11 provide excellent introductions to the theory. Starting with a general n-resonator structure, the equivalent, composite MCF is easily derived by a series of network decompositions as shown in Fig. 7. A filter design having equal inductance values throughout the structure is indicated. As shown in the figure, impedance inverters, having element values corresponding to the shunt capacitances of the structure, have been introduced into the circuit at each of the shunt branch points. Certain sections of the

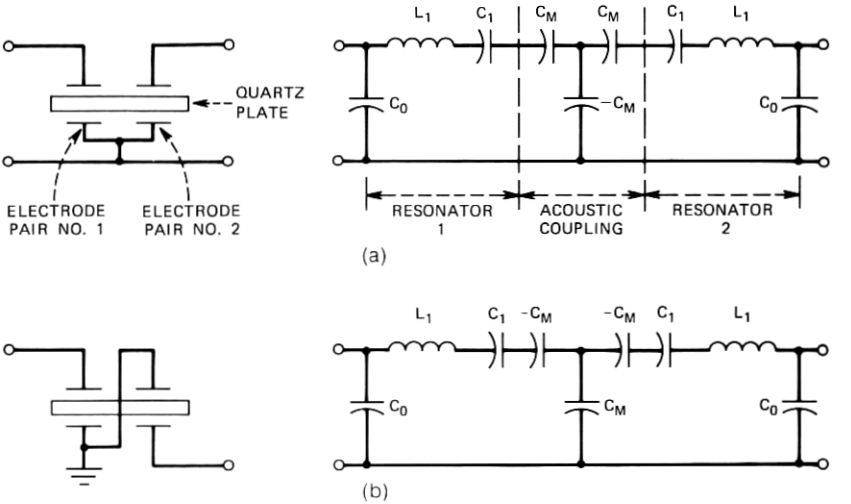

Fig. 5—Schematics and equivalent circuits of monolithic crystal filters. (a) Basic bandpass filter. (b) Reversed-phase bandpass filter.

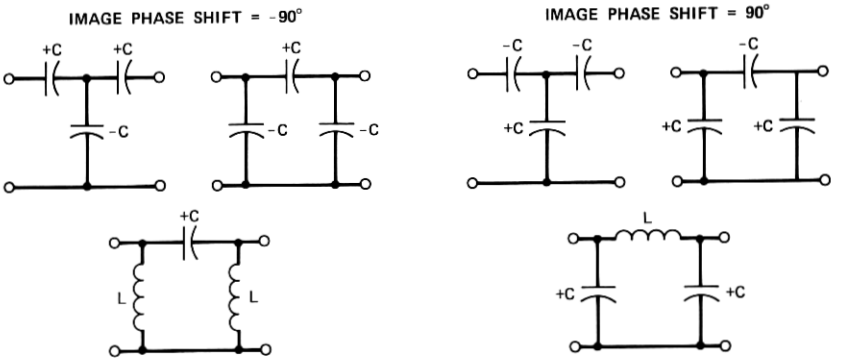

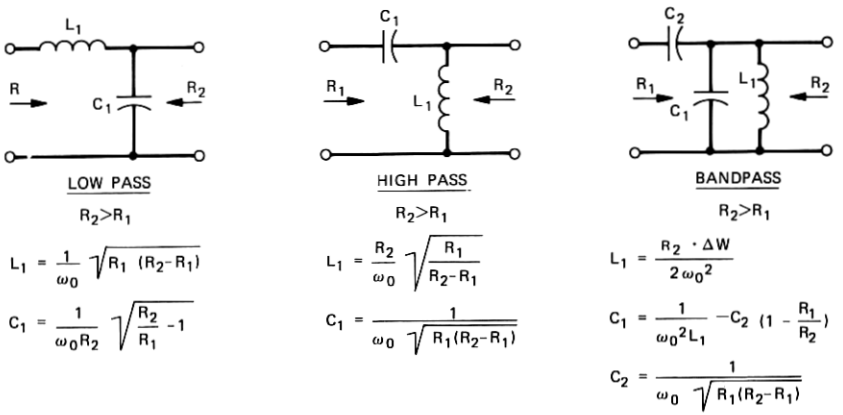

Fig. 6—Narrow-band impedance inverters and impedance-matching networks.

resulting network can be identified as individual, two-resonator MCF's. Impedance inverters coupling the MCF's are also easily identified. If a composite filter design is sought, the impedance inverters indicated in the figure must be changed to their equivalent pi-configurations and the negative capacitance appearing in the series arms replaced by equivalent inductances on a narrow-band approximation basis. The final circuit arrangement is shown in the lower schematic of Fig. 7. It should be noted that, for the composite filter structure comprised of individual two-resonator MCF's, the design must be constrained to an even number of resonators.

The insertion-loss characteristic of a composite monolithic crystal bandpass filter, designed for use as a pick-off filter in the regulating repeater of the L5 system, is shown in Fig. 8.

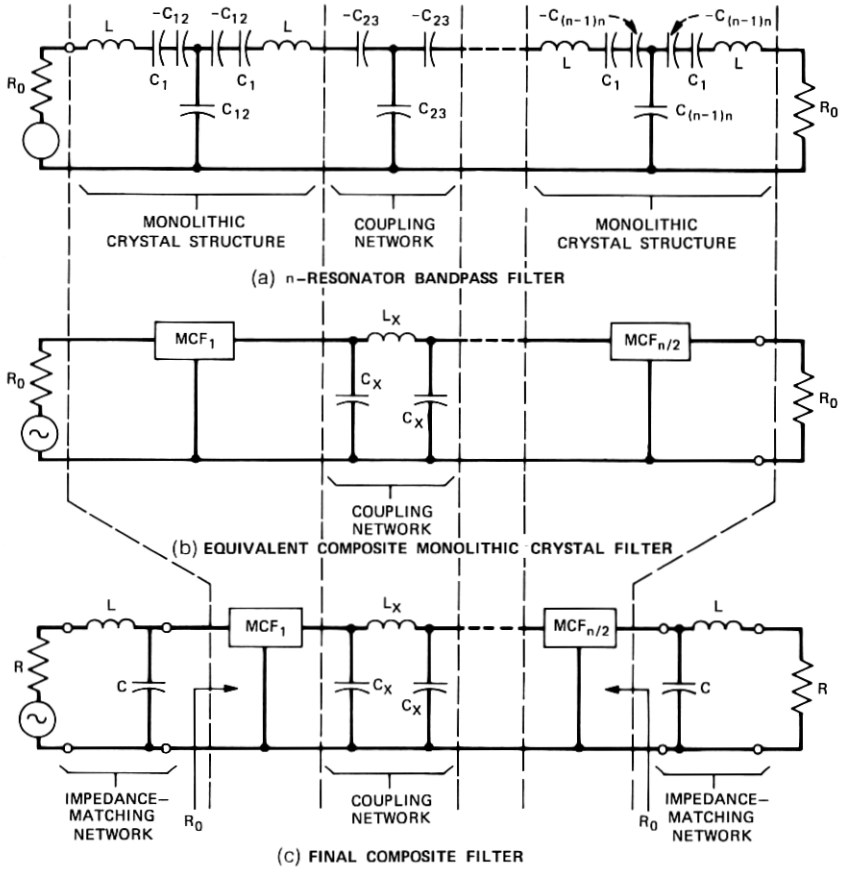

Fig. 7—Decomposition of an n-resonator bandpass filter to an equivalent, composite, monolithic crystal filter structure. (a) n-resonator bandpass filter. (b) Equivalent, composite, monolithic crystal filter. (c) Final composite filter.

1.5 Monolithic crystal band-elimination filters

Although the development of the monolithic crystal bandpass filter was first reported in early 1965, it was not until approximately three years later that the first disclosure of the monolithic band-elimination filter (BEF) was made. Two types of monolithic BEF[12] may be derived from monolithic crystal bandpass filters simply by the addition of inductive or capacitive elements connected across the ungrounded electrodes of conventional two-resonator monolithics. Different connections of the MCF plates, however, must be used to effect proper phase relations in the two types of filter. These phase relations are obtained by use of the basic or the reversed-phase connections previously

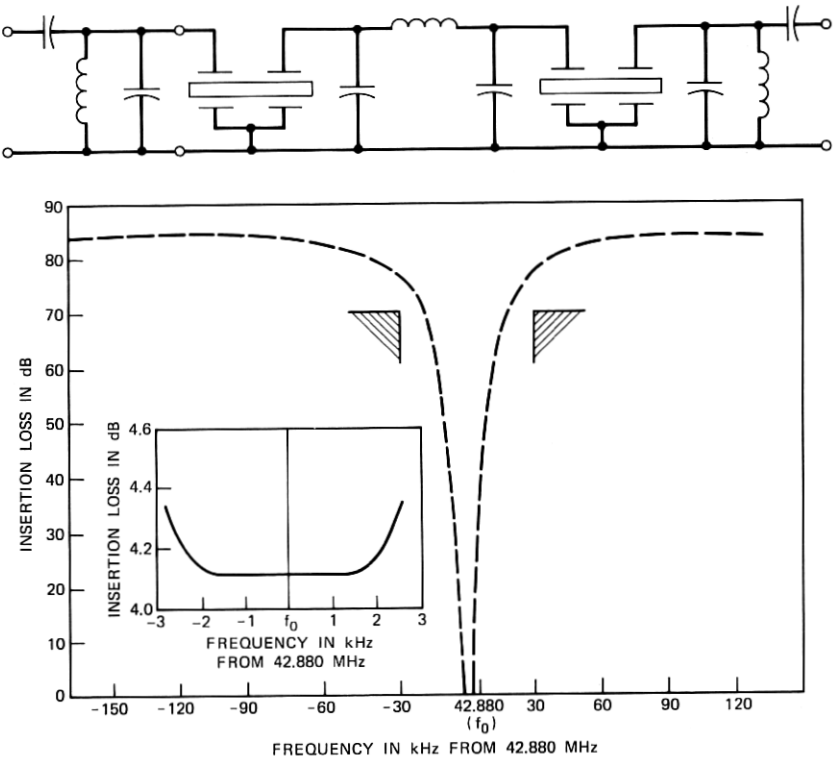

Fig. 8—Example of 42.880-MHz, monolithic crystal, bandpass filter.

shown for the bandpass filter of Fig. 5. Network schematics and equivalent circuits for the inductor- and capacitor-derived BEF's are shown in Fig. 9.

For the inductor-derived filter, the reject frequency occurs when the magnitude of the reactance of the bridging inductor equals that of the acoustic-coupling capacitors of the MCF. This reject frequency occurs at the center frequency of the bandpass filter. For the capacitor-derived filter, the reject frequency is obtained when the magnitude of the bridging capacitance is made equal to that of the acoustic-coupling capacitors.

The band-reject properties of either type of BEF are easily demonstrated by application of Bartlett's bisection theorem. The equivalent lattice of either network is first derived from the open and short-circuited impedances of the bisected network. Combining the redundant elements in the series and lattice arms of the lattice and

plotting reactance as a function of frequency, the passbands and stopbands can be readily identified. For the inductor-derived filter, the insertion loss characteristic includes a passband on either side of a reject band, with a second reject band extending to infinity beyond the second passband. The inductor-derived monolithic BEF is, therefore, a bandstop filter imbedded in a low-pass filter. The capacitor-derived filter, however, is a bandstop filter imbedded in a high-pass structure.

For practical applications, the inductor-derived filter exhibits superior passband performance compared to its capacitor-derived counterpart. Consequently, the remaining discussion of the monolithic BEF will be restricted to the inductor-derived circuit. The initial design procedures, used successfully on both single-section and multi-section monolithic BEF's, were based on dividing the frequency spectrum into two regions: (*i*) the stopband, over which the motional reactances of the MCF change rapidly as the crystal passes through its resonances, and (*ii*) the passband, over which the motional reactances of the MCF are sufficiently high to be considered as open circuits. The extreme stiffness of the resonators makes it possible, therefore, to attribute the frequency response, above and below the narrow stopband, solely to the low-pass filter section of the network. The narrow

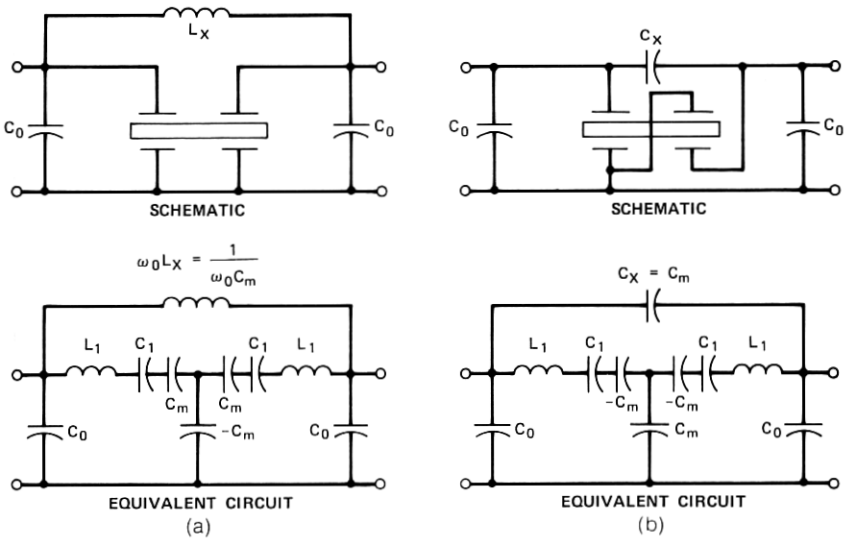

Fig. 9—Monolithic crystal, band-elimination filters. (a) Inductor-derived filter. (b) Capacitor-derived filter.

stopband, however, is controlled by the interactions of the MCF and the bridging inductor.

Single-section and multisection, inductor-derived, monolithic crystal BEF's, shown schematically in Fig. 10, may therefore be designed using standard low-pass synthesis techniques to meet passband requirements. The narrow reject band is formed by adding an estimated number of MCF's, with each monolithic bearing the proper relationship to the corresponding bridging inductor. The stopband performance can then be evaluated from an equivalent-circuit model of the entire network with crystal units being added or removed until the desired characteristic is obtained.

An alternative design technique to that outlined above results in a closed-form synthesis procedure in which a set of filter requirements such as passband ripple, cutoff frequency, and stopband bandwidth are related directly to the set of equivalent circuits shown in Fig. 11. This figure clearly delineates the low-pass and monolithic-crystal sections of the composite filter.

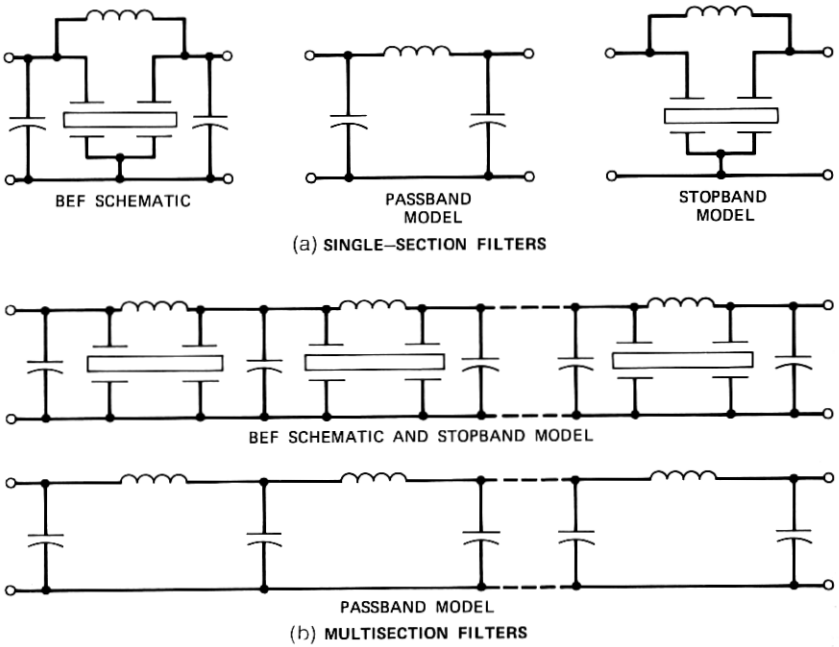

Fig. 10—Inductor-derived, monolithic crystal BEF's. (a) Single-section filters. (b) Multisection filters.

Writing the cascade matrix for each of the component networks of the composite structure, the complete matrix may be formed by converting each of the component matrices to its equivalent admittance form, adding the two resulting matrices and converting the sum back to the cascade form. Such a procedure is essentially routine and provides little insight into the synthesis procedure. If, however, these matrices are expressed in terms of dimensionless parameters[13] and a normalized frequency variable, the elements of a synthesis procedure become apparent. In each instance, the several dimensionless param-

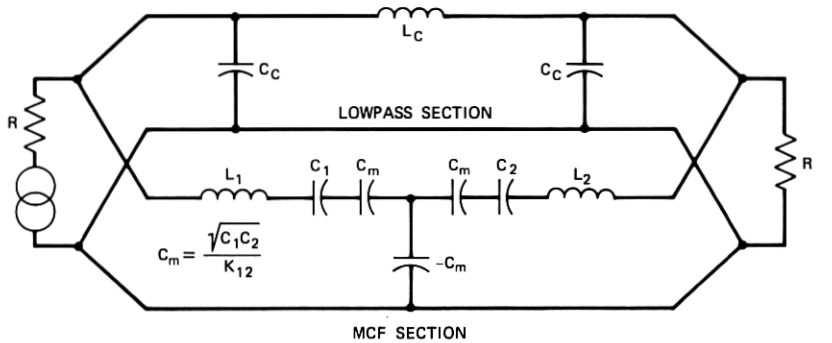

EQUIVALENT CIRCUIT OF INDUCTOR–DERIVED, MONOLITHIC CRYSTAL, BAND–ELIMINATION FILTER

(a)

DIMENSIONLESS PARAMETER	DEFINING NETWORK SECTION
$\epsilon = 1-\omega_0^2 L_C C_C$	LOWPASS FILTER
$D = R/\omega_0 L_C$	LOWPASS FILTER
$r = \omega_0^2 L_C C_m$	BEF (COMBINED ELEMENTS FROM LP AND MCF SECTIONS)
$\bar{L} = (L_1+L_2)/\sqrt{L_1 L_2}$	MCF

NORMALIZED FREQUENCY

Ω/K_{12}, WHERE $\Omega = {}^{f}/_{f_0} - {}^{f_0}/_{f} = 2(f-f_o)/f_0$ *
AND $K_{12} = 1/(\omega_0^2 C_m \sqrt{L_1 L_2})$

* NARROWBAND APPROXIMATION

DIMENSIONLESS PARAMETERS AND DEFINING NETWORK SECTIONS

(b)

Fig. 11—(a) Equivalent circuit of inductor-derived, monolithic crystal, band-elimination filter. (b) Dimensionless parameters and defining network sections.

eters are identified with the component low-pass and MCF's as shown in Fig. 11. The approach described has the further advantage of giving insight into previously unexplained asymmetries that occur in these designs. As a matter of interest, the cascade-matrix approach to network design has also been used to advantage in the design of mechanical filters.[14]

A complete discussion of the cascade matrix approach to the design of composite monolithic crystal BEF's is beyond the scope of the present paper; however, the usefulness of the method in describing seemingly anomalous behavior will be illustrated. A particularly interesting example is that of a two-resonator monolithic BEF having an asymmetric stopband and a Butterworth passband with selected parameters $\epsilon = 0.5$, $D = 1$ (see Fig. 11), and with $f_o < f_{co}$, where f_o is the reject frequency and f_{co} is the cutoff frequency of the low-pass filter. The resulting characteristic of this design is shown in Fig. 12. The solid-line plot is the insertion-loss or stopband model predicted on the basis of the foregoing development. The dashed-line characteristic is that of the Butterworth low-pass filter, and the circled points indicate the characteristic as derived from computer-based mesh analysis of the complete equivalent circuit. Two transition regions are to be noted: the first, below the reject frequency, f_o, and the second, above the reject frequency. In the region below the lower transition region and above the upper transition region, the circled points fall almost exactly on the computed characteristic of the low-pass filter by itself. In the region indicated as the stopband model region, the characteristic predicted by the cascade-matrix method of analysis is duplicated. In the transition regions, however, the approximation is not nearly as good. To simplify the analysis, it was assumed that the reactances of the low-pass filter remained constant in a narrow-band approximation. This approximation breaks down, however, over the transition and passband regions of the BEF. The results of the mesh-analysis computer runs, nevertheless, agree with the predicted characteristic in the stopband to at least three significant figures. The smoothest transition regions are attained in symmetric stopband designs when the reject frequency is placed at an insertion loss zero of a Chebychev low-pass filter. This is illustrated in Fig. 13 for the case of a 0.1579-dB ripple Chebychev passband.

Requirements for some of the BEF's specified for the L5 system included both high-loss stopbands (50 to 80 dB) and very wide passbands (approximately 70 MHz), coupled with low-distortion and high-return-loss requirements. Using Chebychev low-pass filters to

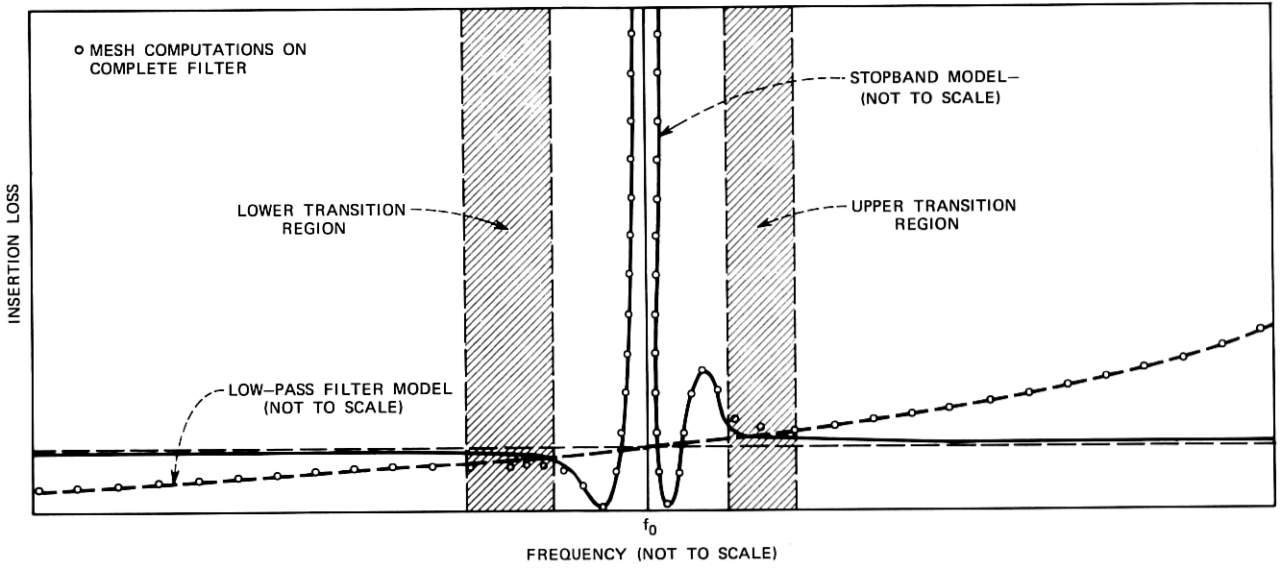

Fig. 12—Characteristic of band-elimination filter with asymmetric stopband and Butterworth passband. Transition regions are indicated ($\epsilon = 0.5$, $D = 1$, $f_o < f_{co}$).

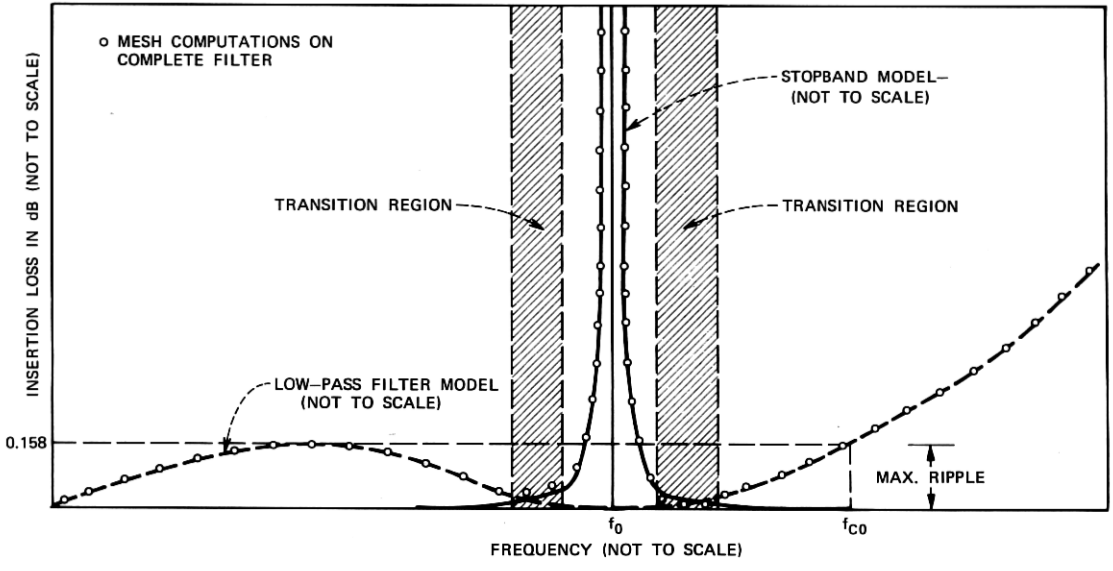

Fig. 13—Characteristic of band-elimination filter with symmetric stopband and 0.1579-dB-ripple Chebychev passband. Transition regions are indicated. Stopband center frequency f_o is at insertion loss zero of the low-pass filter.

model the low-pass section of the composite filter, it was found possible to meet all systems requirements. A specific example of design capability is given in Fig. 14 for a 42.880-MHz BEF, using three two-resonator monolithics imbedded in a ninth-order Chebychev low-pass filter. This low-pass filter was designed at an impedance level of 450 ohms to achieve optimal inductance values for the MCF's. The filter was then matched to the 75-ohm source and load impedances by use of auto-transformers, as shown in the figure. Impedance-matching sections, previously described for bandpass designs, could not be used because of the narrow-band approximations involved. To meet the passband insertion-loss deviation requirements of ±0.05 dB from flat response over the entire frequency range of the L5 system, a simple bridged-T amplitude equalizer was also required.

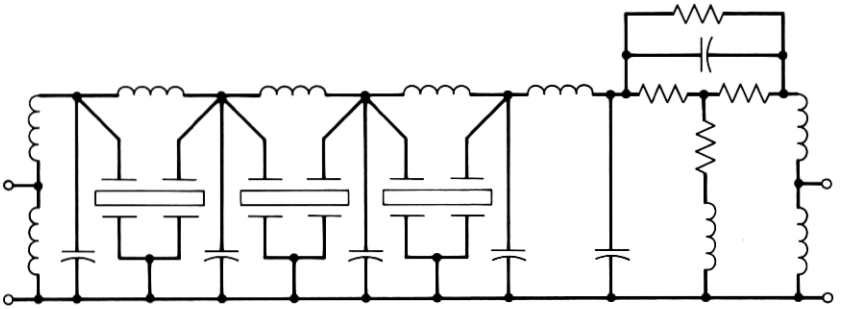

NETWORK SCHEMATIC

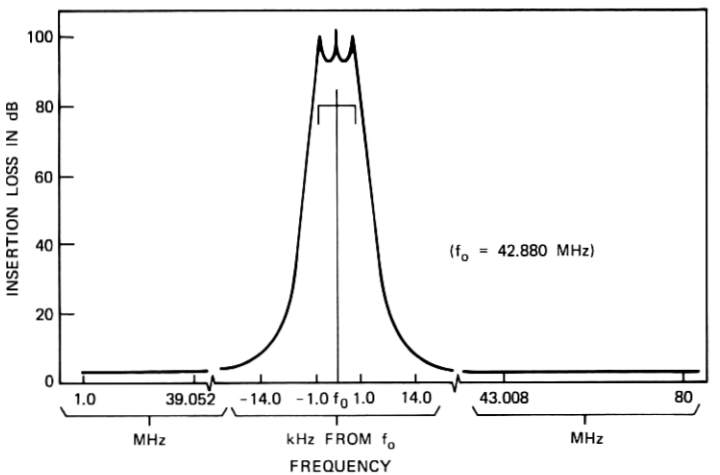

Fig. 14—Example of 42.880-MHz pilot-blocking filter.

1.6 Adjustable Bode equalizers[15,16]

In the L5 coaxial system, a total of 28 adjustable bump shapes are provided to correct for time-invariant amplitude distortions.[17] Ten of these shapes are allocated to the E1 equalizer for coarse correction of distortions introduced by variations in the manufactured product. The remaining 18 shapes are provided by the E2 equalizer to correct whatever residual distortions remain after employment of all lower levels of equalization, including the E1 equalizer.

The majority of bump shapes are realized by series-type, multibump, adjustable Bode equalizers. The remainder are supplied by shaping networks introduced into the feedback paths of isolating amplifiers. The amplifiers buffer the input and output ports of each Bode network and supply gain to offset the losses introduced by the equalizers. Each of the multibump equalizers, however, introduces no more flat loss than would have been introduced by any one of the several single-bump equalizers required to duplicate its performance. With a reduction in the number of Bode networks, the number of isolating amplifiers is also reduced. This, in turn, results in a reduction in intermodulation and thermal noise. Finally, the introduction of shaping networks into the feedback of the isolating amplifiers also reduces the number of Bode networks required. The net effect of all these considerations is to improve reliability, to reduce cost, and as previously indicated, to reduce intermodulation and thermal noise.

All of the multibump Bode networks supplied for the E1 and E2 equalizers were derived from extensions of the simple series-type adjustable network of Fig. 15a. The basic shaping network, as indicated in the figure, is the bridged-T equalizer. Figure 15b shows the range of insertion-loss shapes that may be obtained by variation of load resistor, R_a.

As demonstrated by Lundry,[18] the insertion loss of the generalized Bode network of Fig. 16a can, to a good approximation, be expressed as

$$\theta - \theta_o = \kappa \cdot \rho_a \epsilon^{-2\phi}, \tag{1}$$

where

ϕ = the image transfer constant of the bridged-T network

θ = the insertion loss of the adjustable equalizer

θ_o = the insertion loss of the equalizer when $R_a = R_o$

$\kappa = 2 \tanh \dfrac{\theta_o}{2} = \dfrac{\epsilon^{\theta_o} - 1}{\epsilon^{\theta_o} + 1}$

ρ_a = reflection coefficient of R_a against R_o.

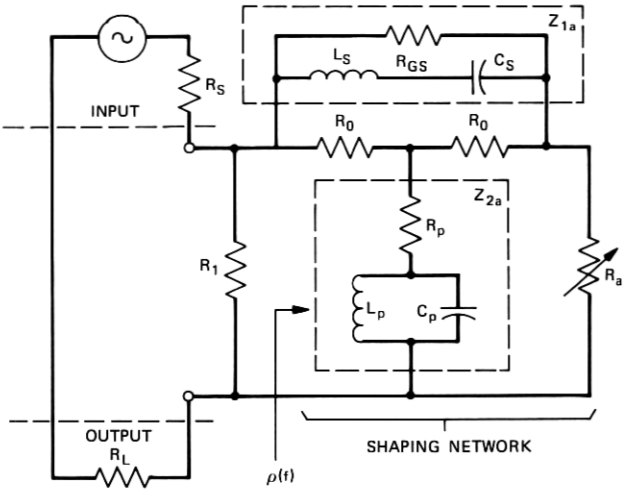

(a)

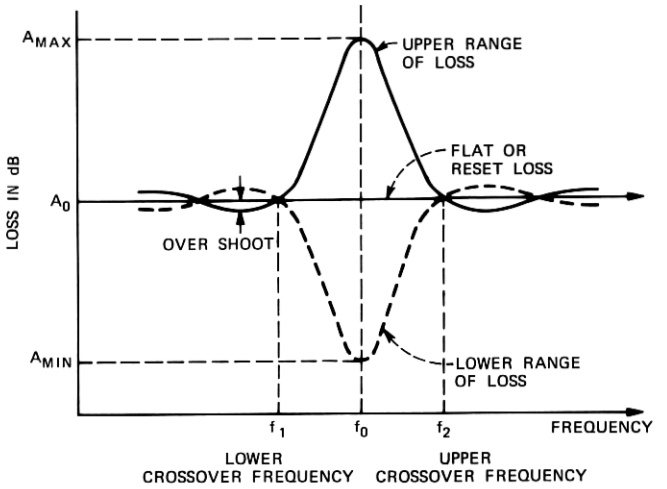

(b)

Fig. 15—Series-type, single-bump, adjustable, Bode equalizer. (a) Schematic. (b) Characteristic.

Equation (1) can also be expressed as

$$\theta - \theta_o = \kappa \cdot \rho(f), \tag{2}$$

where $\rho(f)$ is the input reflection coefficient of the shaping network relative to R_o and is a function of frequency. Considering only the real

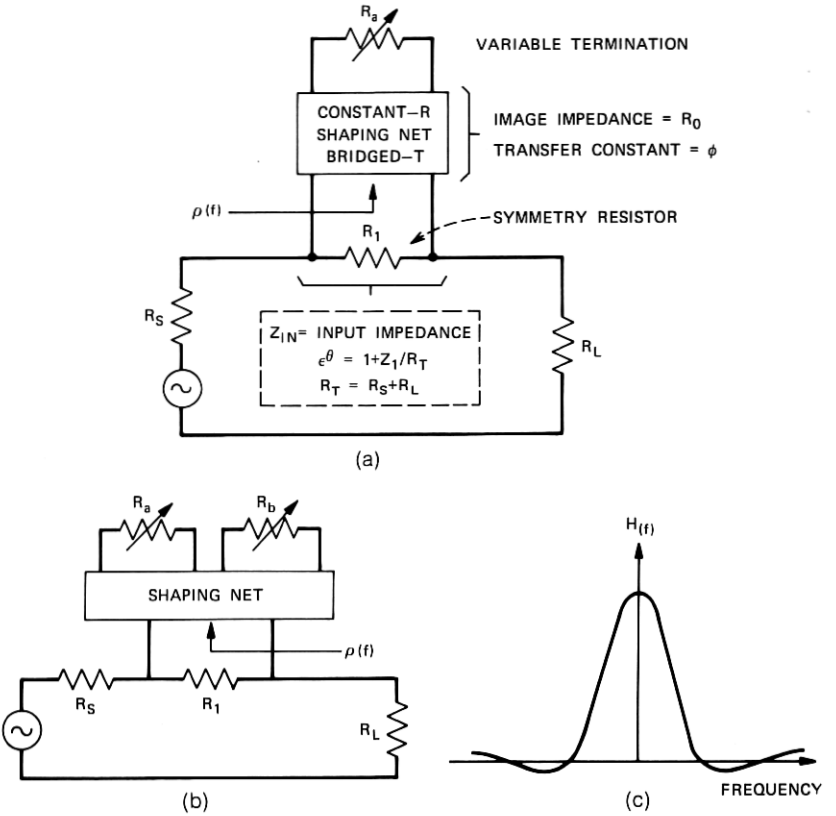

Fig. 16—(a) Series-type, single-bump, Bode equalizer. (b) Series-type, double-bump, Bode equalizer. (c) Bump characteristic, $H(f)$.

part of eq. (2), the insertion loss can be written as

$$\alpha(\text{dB}) = \alpha_o + \text{Re}\,[\kappa \cdot \rho(f)], \tag{3}$$

where α_o is the insertion loss of the structure when $R_a = R_o$. Since α_o and κ are constants, it is only necessary to consider $\rho(f)$.

To realize a single-bump shape with the network of Fig. 16a, Re $|\rho(f)|$ is required to have the form

$$\text{Re}\,|\rho(f)| = H(f)\rho'(R_a), \tag{4}$$

where $H(f)$ is a bump-shaped function of frequency (Fig. 16c), and $\rho'(R_a)$ is a function of a single resistor, independent of frequency.

Similarly, to realize a double-bump shape with the network of Fig. 16b, $\rho(f)$ will have the form

$$\text{Re } |\rho(f)| = H_a(f)\rho_a'(R_a) + H_b(f)\rho_b'(R_b), \tag{5}$$

where the subscripts a and b refer to two separate bump shapes. Both $H_a(f)$ and $H_b(f)$ have the shape indicated in Fig. 16c. For the type of designs discussed here, it is required that these shapes be in distinct frequency bands. R_a and R_b provide independent control of the two shapes.

One method of realizing eq. (5) is to use bridged-T sections as shaping networks. To demonstrate this, a general expression for the input reflection coefficient of a bridged-T network is required. Referring to the schematic of Fig. 17b, which is an unconventional arrangement of the circuit of Fig. 17a, the scattering matrix[19] of the network, with $Z_1 \cdot Z_2 = R_0^2$, is given by

$$\begin{bmatrix} b_1 \\ b_2 \\ b_3 \\ b_4 \end{bmatrix} = \begin{bmatrix} 0 & S_{12}(f) & 0 & S_{14}(f) \\ S_{12}(f) & 0 & S_{14}(f) & 0 \\ 0 & S_{14}(f) & 0 & S_{12}(f) \\ S_{14}(f) & 0 & S_{12}(f) & 0 \end{bmatrix} \cdot \begin{bmatrix} a_1 \\ a_2 \\ a_3 \\ a_4 \end{bmatrix}, \tag{6}$$

where a_i and b_i refer to the incident and reflected voltage waves at the ith port, respectively, and

$$S_{12} = (1 + Z_2/R_o)^{-1}$$
$$S_{14} = (1 + Z_1/R_o)^{-1}.$$

The reflection coefficient $\rho(f) = b_1/a_1$, looking into port 1 of the network, must now be determined. Ports 2 and 4 are terminated in impedances whose reflection coefficients are $\rho_2(f)$ and $\rho_4(f)$, respectively. Assume port 3 is terminated in R_o, and as a result, $\rho_3(f) = 0$.

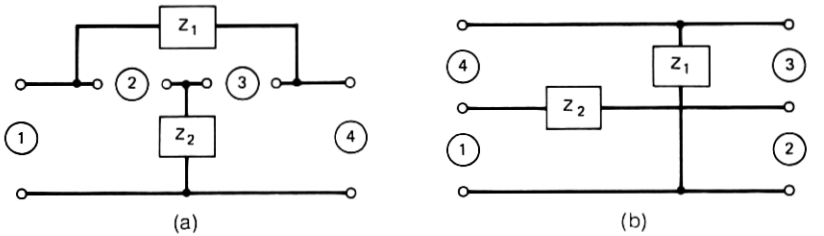

Fig. 17—Bridged-T networks with ports 1 through 4 open-circuited. (a) Conventional. (b) Unconventional.

Thus, the port relationships are

$$\begin{aligned} a_2 &= \rho_2(f)b_2 \\ a_4 &= \rho_4(f)b_4 \\ a_3 &= 0. \end{aligned} \tag{7}$$

These port relationships, together with eq. (6), lead to

$$\rho(f) = S_{12}^2(f)\cdot\rho_2(f) + S_{14}^2(f)\cdot\rho_4(f). \tag{8}$$

Terminating port 2 in R_o and port 4 in R_a leads to

$$\rho(f) = S_{14}^2(f)\rho_4(R_a),$$

where $\rho_4(R_a)$ has been substituted for $\rho_4(f)$, since a resistive element has replaced a frequency-dependent impedance. This has the form of the reflection coefficient for a single-bump shape defined by eq. (4). The single-bump network, based on the unconventional bridged-T network of Fig. 17b, is shown in Fig. 18a.

Because $Z_1\cdot Z_2 = R_o^2$, $S_{12}(f)$ and $S_{14}(f)$ are related by

$$S_{14}(f) + S_{12}(f) = 1. \tag{9}$$

Assume that the shaping network is such that Re $[S_{14}^2(f)]$ is a bump shape centered at frequency f_a. As a result, $S_{14} \approx 1$ in the vicinity of f_a and $s_{14} \approx 0$ elsewhere. From eqs. (8) and (9)

$$\rho(f) = \begin{cases} S_{14}^2(f)\cdot\rho_4(R_a) & \text{(in the vicinity of } f_a\text{)} \\ S_{12}^2(f)\cdot\rho_2(f) & \text{(elsewhere).} \end{cases}$$

In this way, ports 2 and 4 are decoupled.

The term $S_{14}^2(f)\cdot\rho_4(R_a)$ represents a bump shape. As a result, half of the desired equation, (5), has been realized. To realize the second bump shape, $\rho_2(f)$ is made the input reflection coefficient of a similar shaping network whose center frequency is f_b, with $f_b \ll f_a$ or $f_b \gg f_a$. Networks having the assumed properties for S_{14} are shown for a two-bump equalizer in Fig. 18b. For this network,

$$\rho(f) = S_{12a}^2(f)S_{14b}^2(f)\rho_{4b}(R_b) + S_{14a}^2(f)\rho_{4a}(R_a). \tag{10}$$

Equation (10) is now in the proper form to realize the defining equation, (5), of the double-bump equalizer. The equivalence of the two equations becomes apparent when the following substitutions are made in eq. (10):

$$\text{Re}\,[S_{12a}^2(f)\cdot S_{14b}^2(f)]\rho_{4b}(R_b) = H_b(f)\rho_b'(R_b)$$

and

$$\text{Re}\,[S_{14a}^2(f)]\rho_{4a}(R_a) = H_a(f)\rho_a'(R_a).$$

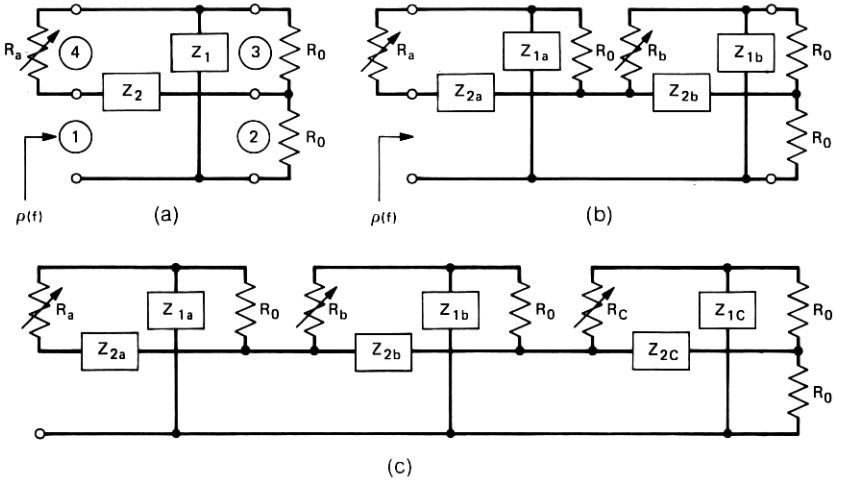

Fig. 18—Shaping network for adjustable bridged-T Bode equalizers. (a) Single bump. (b) Double bump. (c) Triple bump.

The technique described above can be easily extended to the realization of "n" independent bump shapes. The method becomes more or less obvious when the circuit diagrams of Fig. 18a, b, and c, for single-, double-, and triple-bump equalizers are compared.

1.7 Computer-aided network tuning applied to $\sqrt{f}$ regulating network

One of the more recent applications of digital computers is computer-aided tuning of complex networks in manufacture. Without on-line computer adjustment, the $\sqrt{f}$ regulating network of the L5 system could not have been manufactured without relaxation of the performance criteria by a factor of several times. COTMS provided an ideal facility for implementing the alignment algorithm described here.

To compensate for changes in cable loss relative to ground-temperature variations, regulating repeaters are placed in the L5 line approximately every 5 to 7 miles.[17] Relative to nominal cable loss at mean ground temperature, both gain and loss compensation are required according to whether the temperature is above or below mean temperature. In either case, the shape, on a dB (log) basis, is proportional to the square root of frequency. The networks that provide the compensation, as in the L4 system,[20] are thermistor- and pilot-controlled, wideband, square-root-of-frequency Bode networks. They differ from the L4 designs, however, in that buffering amplifiers are included as integral components of the networks, as shown in Fig. 19. Design

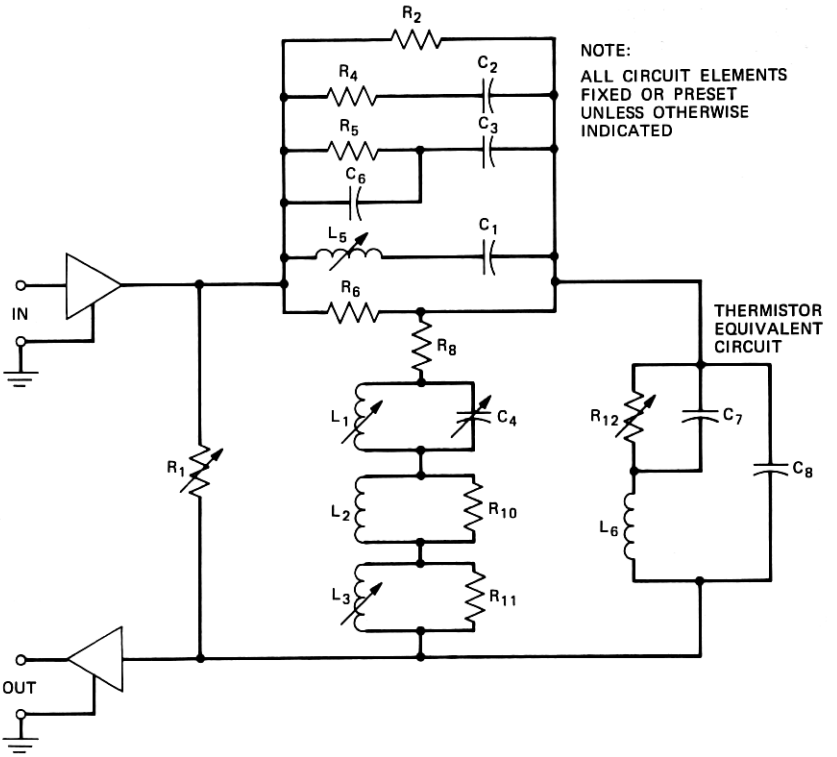

Fig. 19—Simplified schematic of square-root-of-frequency Bode network.

considerations, however, are basically the same and are not reconsidered.

Three measurements are required to fully characterize the network: (*i*) at high-loss setting, (*ii*) at nominal setting, and (*iii*) at low-loss setting (see Fig. 20). The dynamic errors may be defined as

$$e_H(f) = A_H(f) - A_N(f) - K_H\sqrt{f}\ \text{dB} \tag{11}$$

$$e_L(f) = A_L(f) - A_N(f) + K_L\sqrt{f}\ \text{dB}, \tag{12}$$

where $A_H(f)$, $A_N(f)$, and $A_L(f)$ are loss measurements in the high-, nominal-, and low-loss conditions, respectively, and K_H and K_L are determined by requiring the error to be zero, by definition, at the pilot frequency of 42.88 MHz. The static error may be defined as

$$e_N = A_N(f) - A_R(f)\ \text{dB}.$$

$A_R(f)$ is the expected loss in the nominal condition, which, because of parasitics, gain shaping in the amplifiers, and interaction effects, is not flat with frequency. Deviations from the ideal flat shape, however, have the same effect as deviations from the nominal characteristic of other components in the transmission path and may be corrected by fixed and adjustable equalizers available in the system. Since comparable dynamic equalizers are not available, more stringent requirements are placed on the dynamic performance of the Bode equalizer than on the flat or reset shape.

The necessity of requiring three loss measurements, corresponding to three thermistor settings, to characterize network performance, precludes the use of conventional methods for compensating parasitic variations in the amplifiers and the network during manufacture. As it is not possible to guarantee network performance from easily measured amplifier parameters, the alignment procedure must correct for both network and amplifier variations. Since the amplifier is not adjustable, the network must provide tuning capabilities for both shaping and amplifier compensation. Simple prescription of element

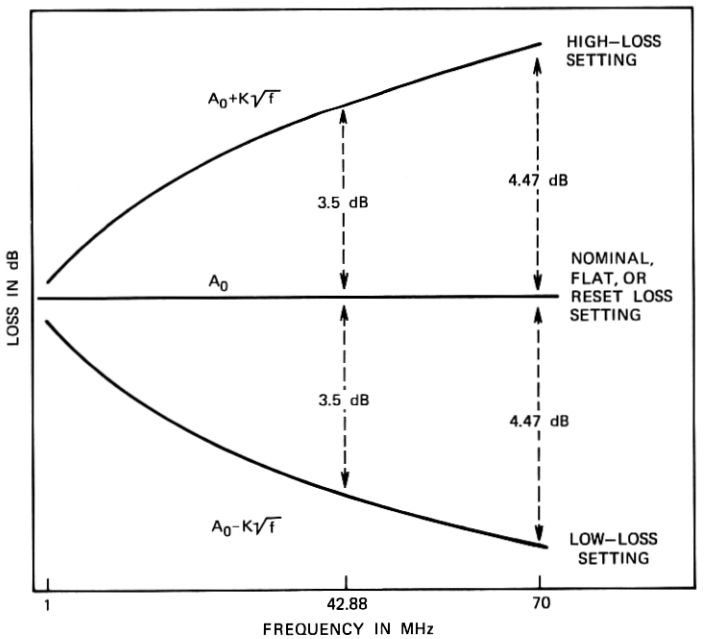

Fig. 20—Square-root-of-frequency Bode-network characteristic.

values or adjustment of resonances would not provide this capability. Furthermore, an adjustment in a network component usually affects all three shapes, making adjustment on a scanner too difficult. Thus, a more sophisticated procedure is needed.

Since the amount of adjustment needed is small, but the allowed deviations even smaller, linearization has proved to be valid. The error after adjustment, $e_{HA}(f)$, can therefore be expressed as:

$$e_{HA}(f) = e_{HI}(f) + \sum_j x_j \Delta_{HJ}(f) \text{ dB}, \tag{13}$$

where $e_{HI}(f)$ is the initial error, $\Delta_{HJ}(f)$ is the normalized deviation caused by the jth component, and x_j is the amount of the deviation used for adjustment. Similar relations hold for the nominal- and low-loss errors. The composite error may be defined as the summed weighted squares:

$$e^2 = \sum_{\text{all } f} [e_H^2(f) + e_L^2(f) + W e_N^2(f)]. \tag{14}$$

A weighting W less than unity allows a larger error in the nominal or reset shape than in the dynamic errors e_H or e_L. Given an initially determined set of errors for the three conditions, over an appropriate frequency band, a set of parameter deviations x_j may be found that minimizes e^2, using the so-called least-sum-of-squares procedure. This procedure is well known and only requires the solution of a set of simultaneous linear equations.

Unfortunately, in practice, the unconstrained solution often requires an adjustment greater than the adjustable components can provide. Thus, it was necessary to include a search for the best constrained solution. The method chosen uses gradient information to determine if a parameter must violate the constraints to lessen the summed-squares error, e^2. Other than being iterative, the method does not require any information beyond that obtained from the least-sum-of-squares procedure. While inclusion of the constraint algorithm contributed to the success of the program in manufacture, a complete description is omitted because of space limitations. It is necessary, of course, to preset the adjustments to a prescribed condition, prior to alignment, to correspond to bounds stored in the program.

Programming for the constrained least-sum-of-squares algorithm was added to a streamlined measurement program for COTMS. The computer controls the measurement sequence and the alignment procedure automatically. The only manual tasks required during tuning are to switch the network into the different conditions and to turn the slugs on the adjustable components. Measured, rather than

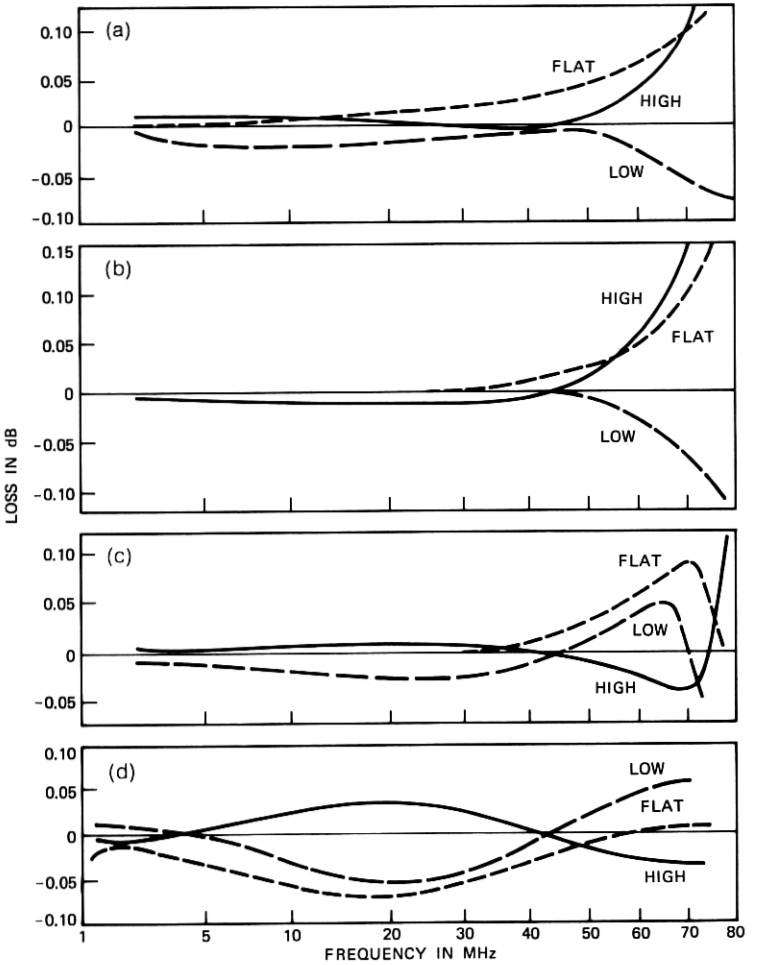

Fig. 21—Deviations in error with element adjustment in square-root-of-frequency Bode network. (a) L1. (b) C4. (c) L5. (d) L3.

computed, deviations from a typical network are used due to the parasitic modeling problem. Because adjustments are effected on a loss basis, it is neither necessary to count turns of the adjustable inductor slugs nor necessary to measure inductance.

The deviations in the high-, nominal-, and low-loss shape errors, caused by variations of four components, are shown in Fig. 21. The curves for inductor L1, for example, show the deviation in the errors corresponding to a 0.1-dB change at 70 MHz in the nominal- or flat-

loss-setting response. The result of the alignment algorithm is a percentage of this deviation. For example, if the multiplier x_j of eq. (13) is determined by the least-sum-of-squares procedure to be 1.32, multiplication of inductor L1 sensitivity (0.1 dB) by this number results in 0.132 dB. Inductor L1 must, therefore, be adjusted for a 0.132-dB change in loss, at 70 MHz, to effect the optimum tuning of that element. For inductor L3, the maximum deviations from flat response occur at approximately 20 MHz over the 1- to 70-MHz frequency range. This inductor is, therefore, tuned at that frequency.

Six adjustable components are included in the program. Only one measurement, adjustment, and remeasurement iteration proved necessary for the adjustment of the networks for optimum performance. "Before" and "after" adjustment error curves are shown in Fig. 22.

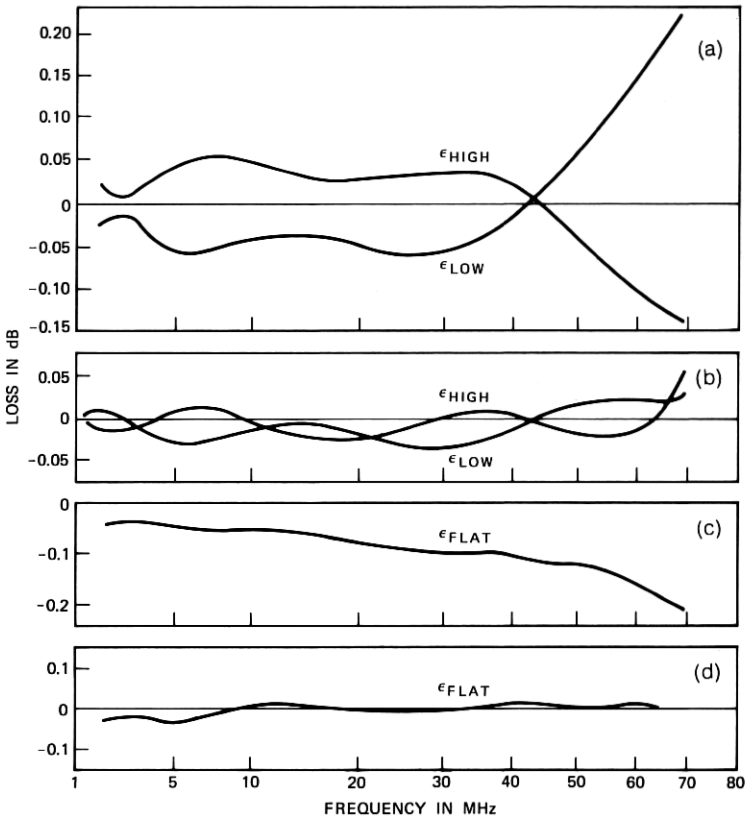

Fig. 22—Network errors before and after adjustment. (a) Before adjustment. (b) After adjustment. (c) Before adjustment. (d) After adjustment.

The computer-aided-adjustment program has proved its value during the several years of manufacture of the regulating network. Without COTMS, this approach would not be feasible. Without computer-aided adjustment, the dynamic regulating objectives for the L5 system could not have been met.

1.8 Deviation equalizers[17]

In a system having as complex an equalization arrangement as L5, the possibility of advantageous interactions among equalizers in the complete hierarchy of equalization must be considered in any one design. An example of such design considerations is the design of the relatively simple, fixed-loss, deviation equalizer. This equalizer compensates for the average error in the match of average-line-repeater gain to nominal cable loss. Three deviation equalizers are installed in each power-feed section.

Initial evaluation of the design led to the conclusion that requirements could be met with an equalizer consisting of two valley-shaped and two bump-shaped bridged-T equalizer sections connected in tandem, as shown in Fig. 23. It was necessary, however, that the design be optimized so that the equalizer, in combination with the E1 and E2 adjustable networks, would provide optimum compensation. This was achieved using the general-purpose optimization program (GPOP) tied together with an E1, E2 simulation program.[21]

The E1, E2 program contains the measured response of all the bump shapes included in the E1 and E2 equalizers. With approximately 15

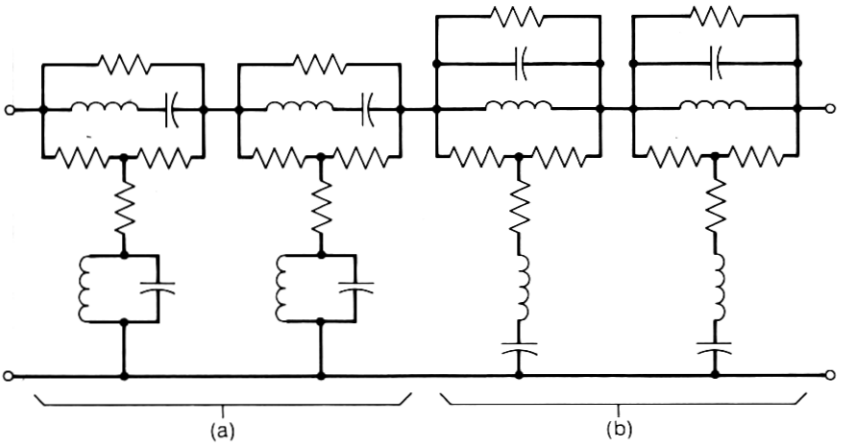

Fig. 23—Deviation equalizer. (a) Valley-equalizer sections. (b) Bump-equalizer sections.

percent of each E1 and E2 bump allotted to the deviation equalizer, optimization resulted in an equalizer characteristic having deviations from ideal placed at frequencies where the E1 and E2 adjustable equalizers could best supply shaping to reduce the overall misalignment.

The E1, E2 simulator package simulated the iterative process that a craftsperson would use in the field in making system equalization adjustments. This yielded an effective design which has led to excellent results on equalized lines.

1.9 Physical design

Although essentially every transmission network for the L5 system provided its own challenges in physical realization, the majority of challenges related to compensation for parasitic inductance and capacitance, to minimization of ground loops, and to reduction of coupling between components. Environmental protection was provided by drawn or fabricated metal enclosures with internally mounted PWB's for supporting and interconnecting the individual circuit components. External connections were, in most instances, made by use of moisture-resistant plugs or jacks.

In several instances, however, substantially greater physical-design effort was involved. Two examples of such design effort are: (*i*) the design of the shaping networks of the line repeaters, and (*ii*) the physical design of the earth-ground filter.

The shaping networks of the basic, regulating, and equalizing repeaters were specifically designed to reduce excess low-frequency gain, to furnish surge protection, and to provide the power-separation filtering requirements of the L5 repeaters. Figures 24a and b show the schematics of the low-frequency A and B networks. The circuit diagrams identify those portions of the networks concerned with the different circuit functions. The network schematic of the bridged-T equalizers used to obtain the desired insertion loss is shown in Fig. 24c.

The physical design of the shaping networks required considerable interaction with system engineers. For overall efficiency and economy of space utilization, the surge-protection and power-separation circuits were included in the shaping-network package. As indicated in the photograph of Fig. 25, the two networks were placed side by side in the lower section of the basic repeater housing. Requirements on RF isolation, between input and output ports of the repeaters, led to the use of cast-aluminum housings for packaging the shaping networks. These housings, in turn, furnished the necessary mechanical

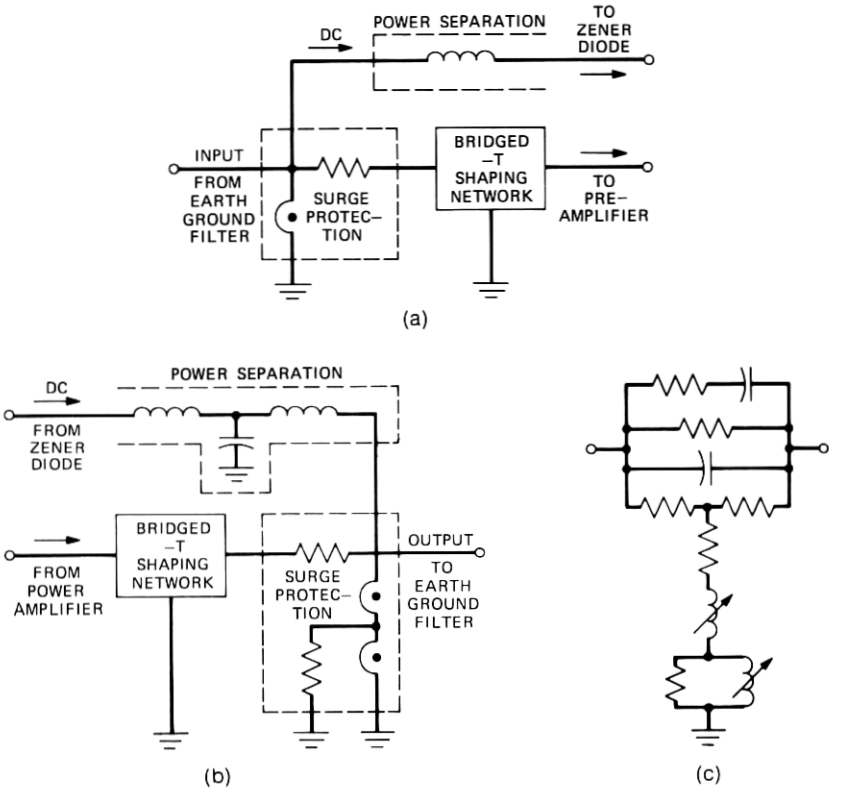

Fig. 24—Low-frequency shaping networks. (a) Network A. (b) Network B. (c) Bridged-T network schematic.

rigidity to meet the ±0.025-dB tolerance on insertion-loss shape as specified for manufacture.

The earth-ground filters of the line repeaters, shown in the photograph of Fig. 25, with their coaxial jacks protruding from the repeater housing, perform several important functions. Despite the seemingly simple electrical circuit shown at the input and output ports of the simplified block diagram of the basic repeater of Fig. 26, the earth-ground filter must

(*i*) Provide high-voltage dc blocking between earth and repeater ground.

(*ii*) Maintain a low-impedance return path between the grounds for all frequencies in the L5 band.

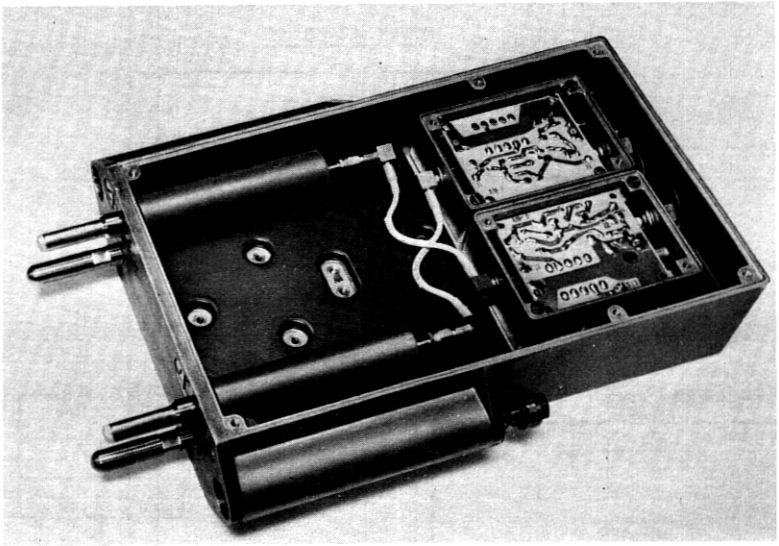

Fig. 25—Earth-ground filters and shaping networks in repeater housing.

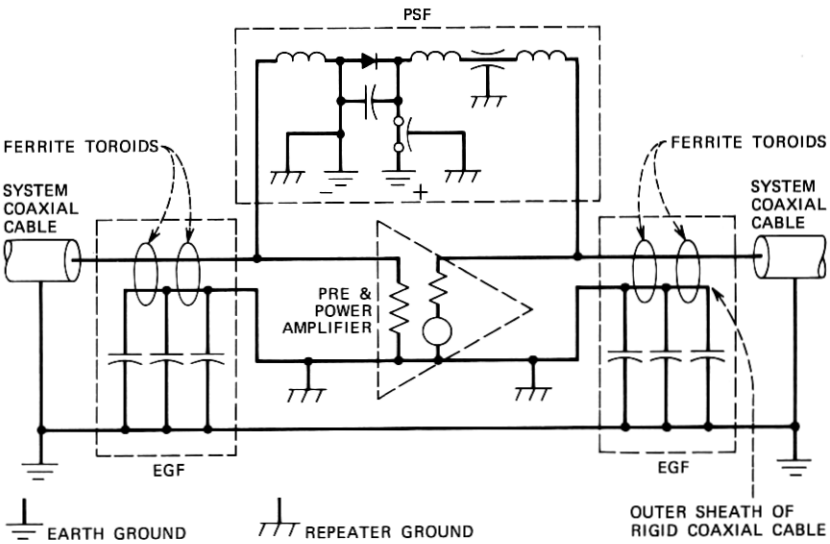

Fig. 26—Block diagram of L5 repeater.

(*iii*) Provide a low-pass filter characteristic with a minimum of 120-dB isolation between repeater input and output (through the ground return) for signals in the L5 band.

(*iv*) Carry the L5 line frequencies and the dc powering current with a minimum of amplitude distortion.

The physical design of the earth-ground filter[22] presented a design challenge. As shown in Fig. 27, the filter contains two coaxial chokes in the form of ferrite toroids and three high-voltage, high-reliability, dual-dielectric capacitors packaged in a sealed enclosure. The filter, minus the coaxial plug, is impregnated with polyisobutylene and hermetically sealed to prevent the entrance of moisture or the leakage of impregnant, which would contaminate the connectors.

To insure the high reliability of this design, considerable emphasis was placed on the compatibility of materials, structural integrity, sealing, and manufacturing control and testing.

II. MAGNETIC COMPONENTS

2.1 Introduction

The L5 system required the development of a wide variety of magnetic components numbering in excess of 100 different experimental designs. This number includes original designs, subsequent improved versions, and redesigns that reflected changing circuit concepts or requirements. Ultimately, about 50 apparatus codes were issued to specify these designs for manufacture. Many additions to existing code series of magnetic components were also made available for L5 applications, but these are not discussed. The adjustable, air-core, precision inductors specified for the manufacture of many of the transmission networks developed for L5 are an example of magnetic component designs based on existing code series.

Coded transformers and inductors appear in all segments of the L5 repeatered line. Frequently, these components are associated with thin-film circuits and, as a result, miniaturized designs had to be made available. Development of inductor structures for such applications, however, predated the development of the L5 system, and, as a result, emphasis is placed here on the development of various types of transformers. Many transformer designs for the line repeaters required pin-type terminals for interconnecting and mounting on PWB's or thin-film substrates. These transformers are discussed in Section 2.2, Repeater Components.

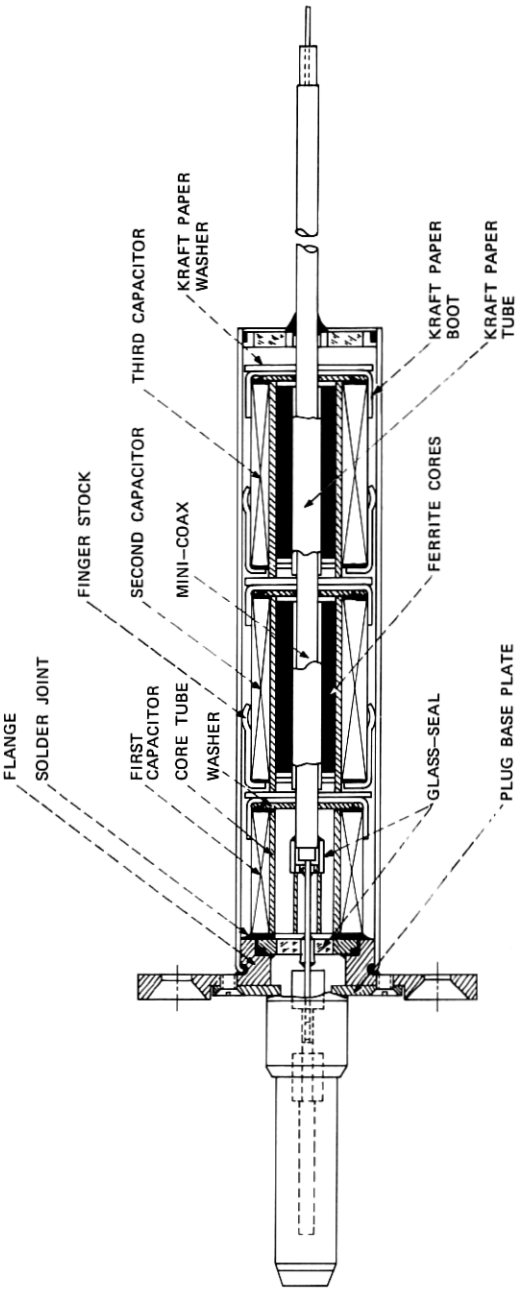

Fig. 27—Cross-sectional view of the earth-ground filter.

Magnetic components intended for terminal applications are frequently used in complex arrays to develop hybrid trees arranged for coaxial interconnection. The different methods used to establish an interface between the magnetic components and the circuitry of the system reflected not only on the problem of physical design, but on the problem of electrical realization as well. Requirements on the individual transformers constituting the hybrid trees had to be tightened to meet overall system performance criteria. As a result, these magnetic components had to be built out with resistors and capacitors to form what are, in effect, special types of transmission networks. Although this type of component is also used to a limited extent in the regulating and equalizing repeaters, a representative design is described in Section 2.3, Terminal Components. Finally, since measurement limitations and techniques were important to all classes of designs, these are discussed separately in Section 2.4.

2.2 Repeater components[17]

The amplifiers in the basic and regulating line repeaters make extensive use of bridge-type feedback,[23] which offers the advantage of making the $\mu\beta$ loop independent of the line impedance Ordinarily, the disadvantages of bridge-type feedback are the extreme impedance levels and the power consumed in the bridge arms used to secure a bridge balance. Both of these limitations, however, may be overcome by use of hybrid transformers. Because of the very tight limits, typically ± 0.02 dB, placed on reproducibility over the 1- to 70-MHz passband, transmission-line design techniques[24] were extensively adapted to the design of hybrid transformers. These designs specify pairs, triplets, or quadruplets of insulated magnet wire twisted uniformly together and wound around a ferrite core. At low frequencies, this arrangement behaves like a conventional transformer, but at high frequencies, where parasitic elements predominate, the device behaves like a transmission line. If the winding inductance and capacitance have been properly proportioned, this approach results in greater bandwidth than can be obtained from a conventional transformer design.

In the case of a two-winding transmission-line transformer operating between equal impedances, the characteristic impedance of the line, $Z_o = \sqrt{L/C}$, should be made equal to the terminating impedance. Under these conditions, the transformer would theoretically have infinite high-end bandwidth. However, the output hybrid of the basic-repeater power amplifier was required to operate between an amplifier

impedance of 50 ohms and a line impedance of 75 ohms with the feedback-port impedance equal to 150 ohms. Since the transmission line used to realize the hybrid could not simultaneously assume all these different values, the best compromise was to make Z_o equal to the geometric mean of the output impedances, or 106 ohms. The ratios of the terminating impedances also forced the use of a trifilar winding. The impedance properties of such windings were studied for various wire gauges, twist rates, insulation thicknesses, and materials. Ultimately, a transmission line made from three strands of AWG 40 polyurethane-insulated wire, combined at a rate of 35 twists per inch, was selected. Although other combinations would have produced the same Z_o, the high twist rate was used because it resulted in the best uniformity from model to model. The schematic diagram and transmission characteristics of the output hybrid are shown in Fig. 28. The divergence in insertion-loss characteristics at high frequencies is the result of the compromise value of impedance selection for Z_o.

Although transmission-line transformers were preferred from a component-design standpoint, they could not always be used because their feedback-port impedance must be an integral multiple of *both* the amplifier and line impedances. To overcome this constraint, conventional layer-wound hybrid transformers were used at the input

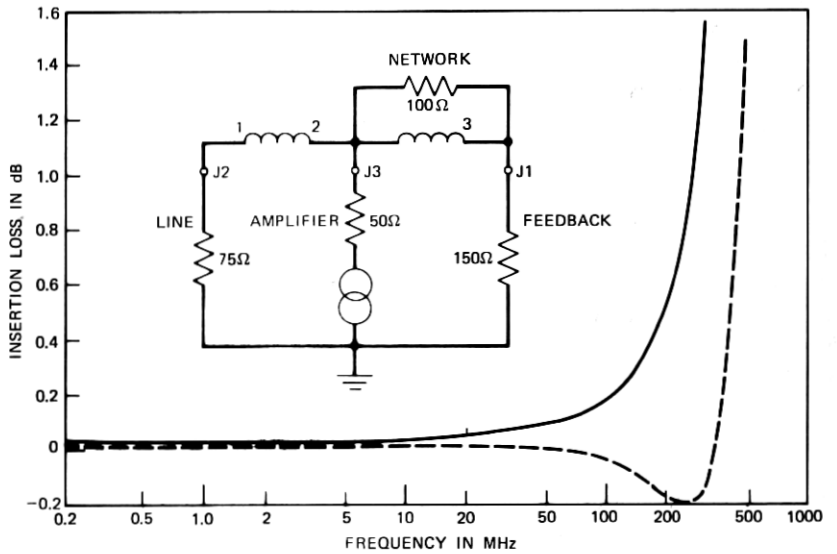

Fig. 28—Schematic and insertion-loss characteristic of output hybrid for basic repeater power amplifier.

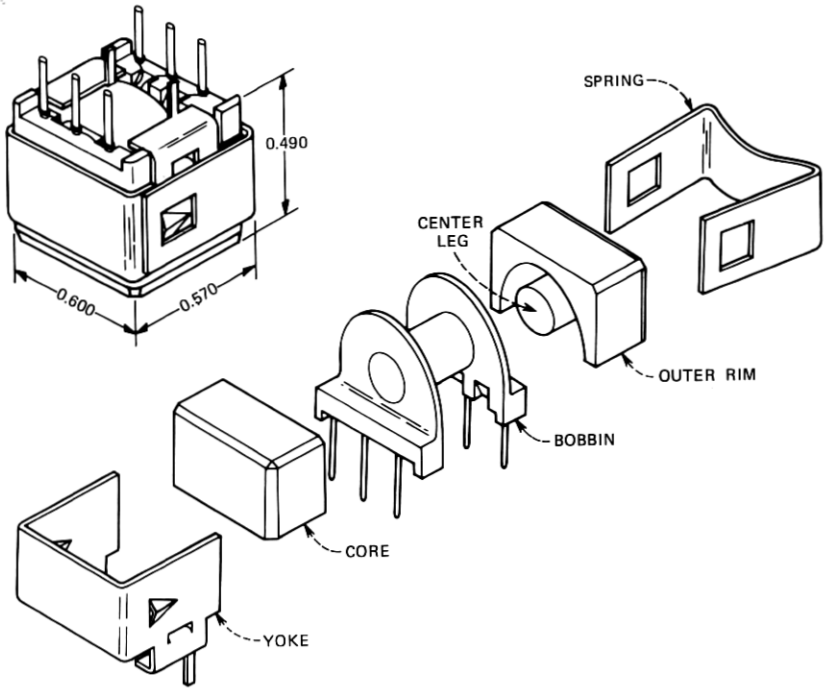

Fig. 29—Transformer structure for conventional layer-wound hybrids using D-cores.

and output of the basic-repeater preamplifier. The initial estimates of the impedances both transformers would be required to match were 75 ohms at the line port, 60 ohms at the amplifier port, and a "low" impedance at the feedback port. Various ratios were evaluated, and the final ratio selected was 75:65 + 28 ohms, which results in a feedback-port impedance of 19.6 ohms.

To provide the best consistency in a layer-wound transformer, a structure that includes a winding bobbin is preferred. Bandwidth considerations, however, dictate that the structure would have to approach the efficiency of a toroid having a winding wrapped directly on the core and extending around its entire periphery. Core and winding dimensions, therefore, are nearly coincident. The D-core shown in Fig. 29 was chosen because the large area of the outer shell produces a low magnetic reluctance. This means that the center-leg length and area control the magnetic properties of the core. Since the winding bobbin fits directly over the center leg, the winding dimensions are only slightly larger than the effective core dimensions, and the structural efficiency approaches that of the toroid.

Evaluation of amplifier models revealed that their high-frequency gains were extremely sensitive to parasitics in the transformer windings. Requirements specified a ±0.02-dB reproducibility from model to model up to 70 MHz. Stringent winding procedures and in-process checks were required to obtain this control in a conventional transformer. Wire gauges and pitches were selected to provide smooth, even, single-layer windings. Carefully controlled paper insulation was used between the most critical windings to insure that the parasitic capacitance could be held to within ±5 percent, which is three times more stringent than normal manufacturing tolerances. Several different types of winding machines were evaluated to obtain one capable of providing the controlled-pitch and constant-tension features required to maintain performance tolerances.

2.3 Terminal components[1,25]

One of the more difficult designs required for terminal applications was a 75:300-ohm, unbalanced-to-balanced transformer intended for use in the JMX modulators. The insertion loss of this transformer was to be held flat to within ±0.1 dB from 0.5 to 70 MHz, and the balance of the center-tapped winding was to exceed 50 dB from 0.5 to 90 MHz. Originally, separate designs were proposed for each jumbogroup because no core material was available that would permit simultaneous realization of these two requirements. In addition, an ability to maintain a balance of the required magnitude over this broad bandwidth had not been demonstrated at these high frequencies. After carefully studying the balance problem, however, it was felt that if an adequate core material could be developed and the mounting structure redesigned, it would be possible to cover the entire range with a single design by employing carefully positioned toroidal windings. The balanced winding consists of seven turns of a bonded pair of wires spaced evenly around the periphery of the core. These windings were then connected in a series-aiding fashion to complete the center-tapped 300-ohm winding. The 75-ohm winding was spaced between adjacent bonded turns and all leads carefully dressed, resulting in a sufficient degree of structural symmetry to maintain the balance. Simultaneously, a new core having the necessary properties was developed and the required mounting structure realized in a new physical design.

Hybrid transformers, to provide combining and splitting functions at a 75-ohm impedance level, were required for several different applications in the L5 system such as LPSS-3, the E3 equalizer, line-connecting arrangements, and JMX circuits. Mounting and coaxial-

connector variations resulted in four distinct physical designs, as shown in the photographs of Fig. 30. The basic electrical building block consists of a transmission-line hybrid and an autotransformer interconnected as shown in Fig. 30a. With reference to that schematic, autotransformer T1 matches the 75-ohm input at jack J1 to the 37.5-ohm impedance at the center tap of hybrid T2. It is wound with a twisted-pair wire whose characteristic impedance $Z_o = \sqrt{75 \times 37.5} = 53.0$ ohms to optimize performance. Since the impedances to be matched differ by 1:2, the tap must be placed at a position corresponding to $1:\sqrt{2}$. This means that the windings cannot consist entirely of twisted-wire transmission line, but must include some free turns. These are created by partially decomposing the twisted bundle, with best results obtained by minimizing the number of free turns.

The hybrid T2 has a 2:1 turns ratio and is wound with a twisted pair having a characteristic impedance of 75 ohms. The network terminating resistance R has a value slightly greater than the ideal 150 ohms to account for transformer core losses, and the capacitor C enhances the high-frequency response of the device. The electrical performance achieved by these components over the 1- to 70-MHz frequency range is as follows: (*i*) the transmission loss from input to either output is 3.10 ± 0.05 dB, (*ii*) the trans-hybrid loss between conjugate output ports is greater than 30 dB, and (*iii*) the return loss at any port is greater than 26 dB. In addition, the two output ports of any individual hybrid track to within 0.02-dB loss and 0.5-degree phase shift. An ideal hybrid would have 3.01-dB transmission loss, infinite trans-hybrid and return losses, and perfect flatness and tracking, with both outputs exactly in phase with each other and the input.

In addition to their use as individual hybrids, particular pairs of these transformers may be grouped to form large n-port arrays or "trees." The transformers in Fig. 30b use standard Bell System coaxial plugs and jacks so arranged that they may be interconnected directly. The transformers in Fig. 30c use miniature coaxial connectors and may be formed into trees by cabling them together. To reduce the number of interconnections required, the hybrid at the right of Fig. 30c, a dual hybrid, has an input, one -3-dB output, and two -6-dB outputs. The hybrid at the left of Fig. 30c is a single hybrid of the type shown in Fig. 30a.

2.4 Transmission measurements

The ± 0.02-dB reproducibility of insertion loss required for many L5 magnetic-component designs could not be guaranteed initially by direct measurements because neither the test set nor the apparatus

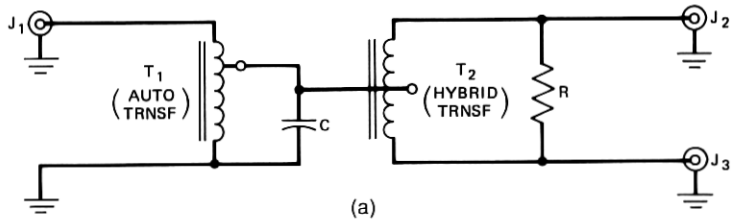

(a)

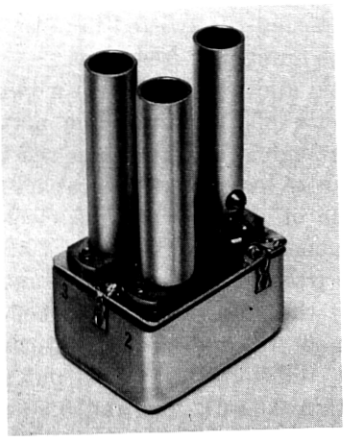

SINGLE HYBRID
(THREE–JACK DESIGN)

(b)

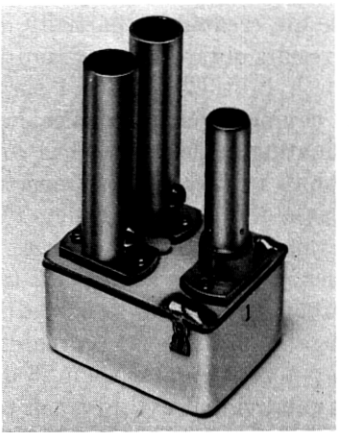

SINGLE HYBRID
(TWO–JACK, ONE–PLUG DESIGN)

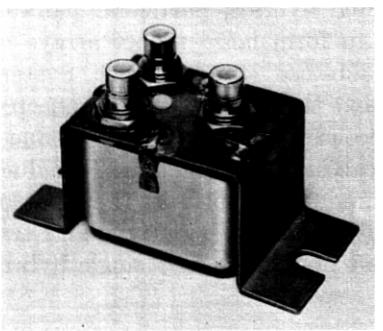

SINGLE HYBRID
(THREE–JACK DESIGN)

(c)

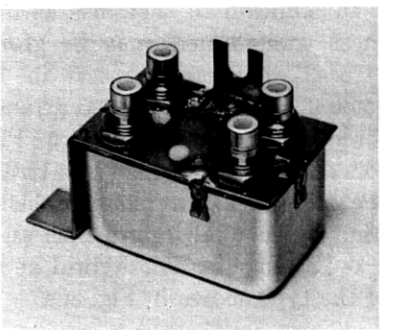

DUAL HYBRID
(FOUR–JACK DESIGN)

Fig. 30—Hybrid transformers for L5 terminals. (a) Building-block schematic. (b) Hybrids with Bell System coaxial connectors. (c) Hybrids with miniature coaxial connectors.

under test exhibited a return loss compatible with this extremely tight limit. Instead, a system was used in which a set of transformers known to have the proper characteristics in an amplifier was used to calibrate a test fixture. The calibrated fixture was then used to measure product. To guard against changes in the fixture or measurement system, however, these measurements were correlated to those made on reference transformers whose histories were well known. When either fixtures or reference units needed replacement, the appropriate steps in the calibration and correlation processes were repeated. Meanwhile, a program to provide improved measurement capability for these devices was begun.

To have a reproducible base line for loss measurements on COTMS,[3] a simple strap between the transformer input and output ports of the test fixture was used. While this introduces reflections because these ports often have different impedances, it is the simplest and most consistent method of eliminating differences in test sets, connectors, and cables. Furthermore, with sufficient padding close to the COTMS ports of the fixture, satisfactory base-line reproducibility can be obtained. Accordingly, alternate measurement schemes were discarded in favor of upgrading the existing approach.

The test fixtures were originally constructed with ordinary PWB's. The contacts to the pin-type transformer terminals were made with miniature spring sockets, and the interconnection to the test set used Bell System coaxial connectors. The resistive pads used to match the transformer impedances to the COTMS ports were made with various types of discrete resistors for the different transformer codes. It was recognized very early that the required reproducibility of measurements would be difficult to maintain in a production environment with this type of test fixture. Coaxial connectors can introduce impedance discontinuities, and spring sockets can become contaminated or wear out with frequent use. When replaced, resistive pads are often damaged by the heat of soldering and change value. In addition, the associated parasitic electrical element values are a function of exact mechanical configuration and placement which are difficult to control.

Improved designs of the spring contacts and of the coaxial connectors were introduced to improve the performance of the test fixtures. Knife-edge contacts with force-free insertion were used to replace the former, while the latter were superseded by precision 50-ohm versions. As the next step, the PWB was replaced by an alumina substrate having controlled dielectric properties. Tests quickly indicated new problems. Because of the higher dielectric constant of the substrate,

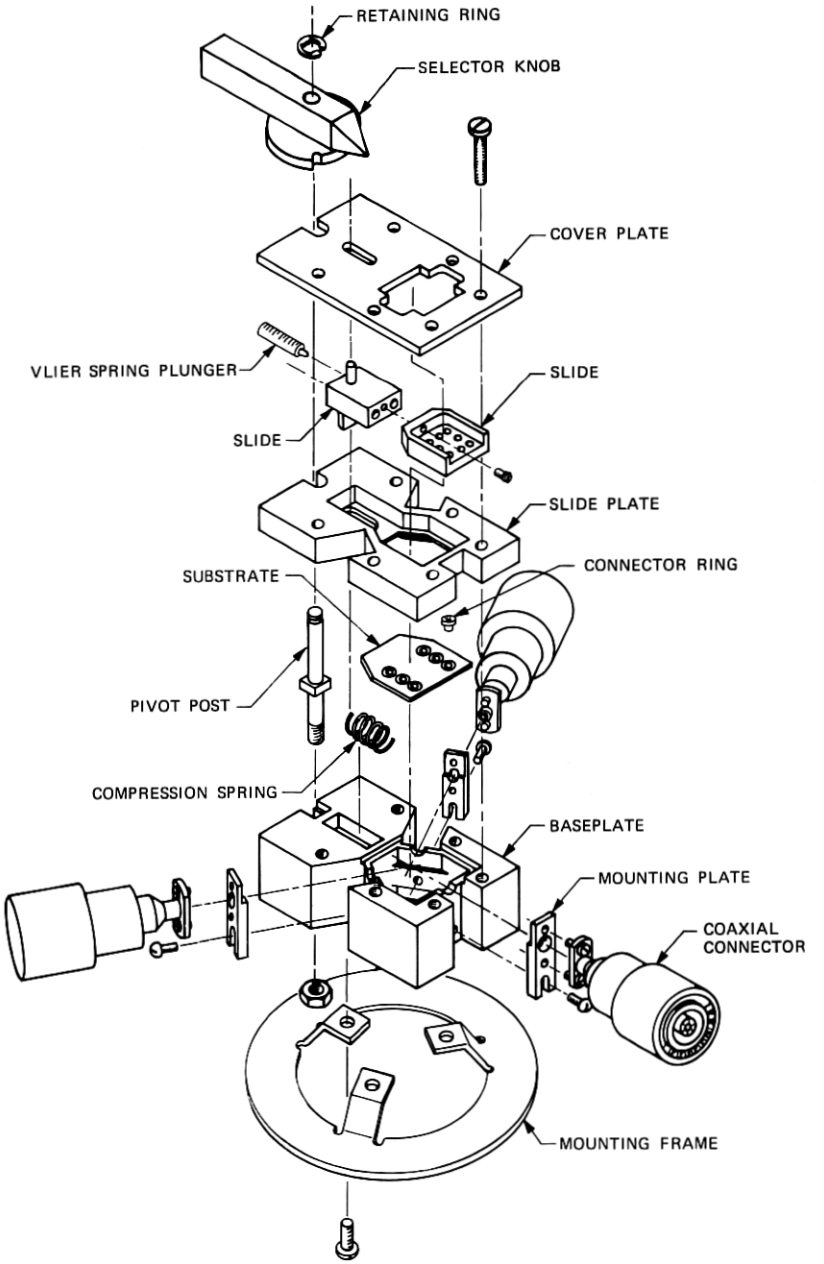

Fig. 31—L5 transformer test fixture.

the effective electrical length of the connections increased significantly, causing difficulty with crosstalk and reflections. The chip resistors, which were chosen for the matching pads, changed value on soldering and caused reproducibility and rework difficulties. A final design evolved in which the path lengths of the microstrip connections on the substrate were reduced to a minimum and the resistors realized as thin-film elements. This arrangement permits high accuracy in the adjustment of resistance values, makes parasitic elements closely reproducible, and eliminates the repair operations that had been required with the original fixture design. External connection problems were further reduced by coupling the coaxial connectors to the substrate via precision spring-loaded microstrip launchers. These new fixtures, shown in the exploded view of Fig. 31, have attained a reproducibility of better than ± 0.01 dB.

III. CONCLUSION

Transmission networks and magnetic components are among the least visible components of the L5 system. Despite this lack of visibility, these components serve vital systems functions. Many of these functions are reviewed in this paper. The principal objectives of the paper, however, are to record those state-of-the-art advances that have contributed to the success of the L5 system, and to identify those allied technologies that have influenced network and magnetic component development. The influence of the computer in analysis and synthesis, precision measurement, and optimization is stressed, and the added influence of development in the piezoelectric device and magnetic materials areas has been noted. In many instances, developments in these allied technologies predated the L5 system and resulted from a general philosophy of "tool building" initiated, specifically, to have these technologies keep pace with future systems and component-development needs. Without such a philosophy, L5 requirements could not have been met on schedule.

IV. ACKNOWLEDGMENTS

Many individuals, too numerous to mention, have made significant contributions to the development of transmission networks and magnetic components for the L5 system. These contributions have come from individuals in the authors' own departments and from co-workers at other Bell Laboratories locations. Special thanks, however, must be given to R. L. Adams and G. J. Mandeville for contributing to the sections on computer-aided tuning of networks and the design of multibump, adjustable Bode equalizers, respectively.

REFERENCES

1. R. E. Maurer, "L5 System: Jumbogroup Multiplex Terminal," B.S.T.J., this issue, pp. 2065–2096.
2. G. Szentirmai, "A Filter Synthesis Program," in *System Analysis by Digital Computer*, ed. F. F. Kuo and J. F. Kaiser, New York: J. Wiley and Sons, 1966, pp. 130–174.
3. W. J. Geldart, G. D. Haynie, and R. G. Schleich, "A 50-Hz to 250-MHz Computer Operated Transmission Measuring Set," B.S.T.J., *48*, No. 5 (May–June 1969), pp. 1339–1381.
4. R. A. Sykes, W. L. Smith, and W. J. Spencer, "Monolithic Crystal Filters," IEEE International Convention Record, 1967, pp. 79–93.
5. W. G. Alberts, J. B. Evans, T. J. Haley, T. B. Merrick, and T. H. Simmonds, Jr., "L4 System: Terminal Arrangements," B.S.T.J., *48*, No. 4 (April 1969), pp. 1024–1025.
6. J. L. Garrison, A. N. Georgiades, and H. A. Simpson, "The Application of Monolithic Crystal Filters to Frequency Selective Networks," Digest of Technical Papers, 1970 International Symposium on Circuit Theory, 1970, pp. 177–178.
7. H. A. Simpson, E. D. Finch, Jr., and R. K. Weeman, "Composite Filter Structures Incorporating MCFs and LC Networks," Proceedings of the 25th Annual Symposium on Frequency Control, Fort Monmouth, N.J.: U. S. Army Electronics Laboratories, 1971, pp. 287–290.
8. P. Lloyd, "Monolithic Crystal Filters for Frequency Division Multiplex," ibid., pp. 280–286.
9. M. Dishal, "Two New Equations for the Design of Filters," Electrical Communication, *30*, December 1952, pp. 324–337.
10. A. I. Zverev, *Handbook of Filter Synthesis*, New York: J. Wiley and Sons, 1967, Chapter 6.
11. "Filters, Modern Network Theory Design," *Reference Data for Radio Engineers*, ed. H. P. Westman, Fifth Edition, ITT, 1968, Chapter 8.
12. J. L. Garrison and A. N. Georgiades, "Band-Elimination Filters," U. S. Patent 3,704,433, November 28, 1972.
13. A. A. Comparini, "Analysis and Synthesis of a Band-elimination Filter Using Monolithic Crystal Filters," unpublished memorandum.
14. L. Brier, "Der Entwurf von HF-Bandfiltern und Mechanischen Filtern mit Dampfungspolen nach dem Betriebsparameterverfahren," Guest Lecture at the International Science Colloquium, University of Ilnienan, September 1965.
15. H. W. Bode, "Variable Equalizers," B.S.T.J., *17*, No. 2 (April 1938), pp. 229–244.
16. F. C. Kelcourse, W. G. Scheerer, and R. J. Wirtz, "L4 System: Equalizing and Main Station Repeaters," B.S.T.J., *48*, No. 4 (April 1969), pp. 907–911.
17. E. H. Angell, Y.-S. Cho, K. P. Kretsch, and M. M. Luniewicz, "L5 System: Repeatered Line," B.S.T.J., this issue, pp. 1935–1985.
18. W. R. Lundry, "Attenuation and Delay Equalizers for Coaxial Lines," Transactions of AIEE, *68*, 1949, pp. 1174–1179.
19. H. J. Carlin, "The Scattering Matrix in Network Theory," IRE Transactions on Circuit Theory, *CT-3*, No. 2 (June 1956), pp. 88–97.
20. J. L. Garrison, L. P. Labbe, and C. C. Roch, "Basic and Regulating Repeaters," B.S.T.J., *48*, No. 4 (April 1969), pp. 871–876.
21. R. M.-M. Chen, C. F. Hempstead, Y. L. Kuo, M. L. Liou, R. P. Snicer, and E. D. Walsh, "L5 System: Role of Computing and Precision Measurements," B.S.T.J., this issue, pp. 2249–2267.
22. R. A. Thatch and F. D. Waldhauer, "High Frequency Ground Isolation Filter for Line Powered Repeater Circuits," U. S. Patent No. 3,530,393, September 22, 1970.
23. H. W. Bode, *Network Analysis and Feedback Amplifier Design*, Princeton, N.J.: D. Van Nostrand Company, 1945, Chapter III, pp. 37–38.
24. C. L. Ruthroff, "Some Broadband Transformers," Proc. IRE, *47*, No. 8 (August 1959), pp. 1337–1342.
25. R. K. Bates and D. J. Zorn, "L5 System: Signal Administration and Interconnection," B.S.T.J., this issue, pp. 2129–2145.